White Rose Research Online

eprints@whiterose.ac.uk
https://eprints.whiterose.ac.uk
Universities of Leeds, Sheffield and York

Deposited via The University of Leeds.

White Rose Research Online URL for this paper:
https://eprints.whiterose.ac.uk/id/eprint/119723/

Version: Accepted Version

Article:
Kempf, A, Boda, E, Kwok, JCF et al. (2017) Control of cell shape, neurite outgrowth and migration by a novel Nogo-A/HSPG interaction. Developmental Cell, 43 (1). pp. 24-34. ISSN: 1534-5807

https://doi.org/10.1016/j.devcel.2017.08.014

© 2017 Elsevier Inc. This manuscript version is made available under the CC-BY-NC-ND 4.0 license http://creativecommons.org/licenses/by-nc-nd/4.0/.

Reuse
Items deposited in White Rose Research Online are protected by copyright, with all rights reserved unless indicated otherwise. They may be downloaded and/or printed for private study, or other acts as permitted by national copyright laws. The publisher or other rights holders may allow further reproduction and re-use of the full text version. This is indicated by the licence information on the White Rose Research Online record for the item.

Takedown
If you consider content in White Rose Research Online to be in breach of UK law, please notify us by emailing eprints@whiterose.ac.uk including the URL of the record and the reason for the withdrawal request.

UNIVERSITY OF LEEDS
University of Sheffield
UNIVERSITY of York

Control of cell shape, neurite outgrowth and migration by a novel Nogo-A/HSPG interaction

Anissa Kempf[1#], Rafael Fritz[2], Enrica Boda[3], Jessica C.F. Kwok[4&], Valentina Grande[3], Andrea M. Kaelin[1], Zorica Ristic[1], Andre Schmandke[1], Antonio Schmandke[1], Björn Tews[5], James W. Fawcett[4], Annalisa Buffo[3], Olivier Pertz[2*], Martin E. Schwab[1]

[1] Brain Research Institute, University of Zurich, and Department of Health Sciences and Technology, Swiss Federal Institute of Technology (ETH) Zurich, Winterthurerstrasse 190, CH-8057, Zurich, Switzerland

[2]Institute for Biochemistry and Genetics, Department of Biomedicine, University of Basel, CH-4058, Basel, Switzerland

[3] Department of Neuroscience, Neuroscience Institute Cavalieri Ottolenghi (NICO), Università degli Studi di Torino, Regione Gonzole, 10-10043, Orbassano (Turin), Italy

[4]John van Geest Centre for Brain Repair, Department of Clinical Neurosciences, University of Cambridge, Robinson Way, Cambridge CB2 0PY, United Kingdom

[5]Schaller Research Group at the University of Heidelberg and the German Cancer Research Center (DKFZ), Molecular Mechanisms of Tumor Invasion, 69120 Heidelberg, Germany

*Present address: Institute of Cell Biology, University of Bern, Baltzerstrasse 4, CH-3012 Bern, Switzerland

[&]Present address: School of Biomedical Sciences, Faculty of Biological Sciences, University of Leeds, Leeds LS2 9JT, United Kingdom

[#] Lead contact.

Corresponding authors:

Martin E. Schwab, schwab@hifo.uzh.ch, and Anissa Kempf, anissa.kempf@cncb.ox.ac.uk

Address: Brain Research Institute, University of Zurich and Department of Health Sciences and Technology, Swiss Federal Institute of Technology, Winterthurerstrasse 190, 8057 Zurich,Switzerland

Tel direct: +41446353330, and Fax: +41446353303

Lead contact: Anissa Kempf (anissa.kempf@cncb.ox.ac.uk)

Summary

Heparan sulfate proteoglycans (HSPGs) critically modulate adhesion-, growth- and migration-related processes. Here we show that the transmembrane protein Nogo-A inhibits neurite outgrowth and cell spreading in neurons and Nogo-A-responsive cell lines via HSPGs. The extracellular, active, 180 aa Nogo-A region called Nogo-A-Δ20 binds to heparin and brain-derived heparan sulfate glycosaminoglycans (GAGs) but not to the closely related chondroitin sulfate GAGs. HSPGs are required for Nogo-A-Δ20-induced inhibition of adhesion, cell spreading, neurite outgrowth as well as for RhoA activation. Surprisingly, we show that Nogo-A-Δ20 can act via HSPGs independently of its receptor Sphingosine-1-Phosphate receptor 2 (S1PR2). We thereby identify a new functional binding receptor for Nogo-A-Δ20 and show that syndecan-3 and syndecan-4 are responsible for Nogo-A-Δ20-induced effects. Finally, we show in explant cultures ex vivo that Nogo-A-Δ20 promotes the migration of neuroblasts via HSPGs but not S1PR2.

45 **Keywords**

46 Nogo-A, HSPG, outgrowth, spreading, adhesion, neuroblast, migration, SVZ, RMS

Introduction

Cell surface heparan sulfate proteoglycans (HSPGs) are highly expressed in the mammalian nervous system (Sarrazin et al., 2011; Yamaguchi, 2001). HSPGs regulate various developmental processes ranging from neuroblast migration, axon growth and guidance to synapse formation and neuronal connectivity (Inatani et al., 2003; Van Vactor et al., 2006; Yamaguchi, 2001). HSPGs transduce signals originating in the extracellular matrix (ECM) or act as obligate co-receptors for several morphogens, growth factors and axon guidance molecules (Bernfield et al., 1999; Sarrazin et al., 2011). Most studies on HSPGs have focused on the regulation of survival-, proliferation- or growth-promoting cues, e.g., fibroblast growth factor (FGF) (Sarrazin et al., 2011), rather than growth-inhibiting and repulsive factors. To our knowledge, only the repulsive activities of EphrinA3, Slit2 and S1P have been reported to critically depend on the presence of cell surface HSPGs so far (Hu, 2001; Irie et al., 2008; Strochlic et al., 2008).

Nogo-A is a major anti-adhesive and neurite growth-inhibitory protein initially discovered for its role as myelin-associated inhibitor of axonal regeneration in the adult central nervous system (CNS) (Schwab, 2010). In addition to its role in the injured CNS, Nogo-A has been shown to regulate various developmental and plastic processes ranging from synapse formation to neuronal migration (Kempf and Schwab, 2013; Schwab and Strittmatter, 2014). In the adult brain, Nogo-A promotes cell motility and the tangential migration of neuroblasts along the rostral migratory stream (RMS) by triggering cell-cell repulsion (Rolando et al., 2012). At hippocampal and cortical synapses, Nogo-A acts as a negative regulator of long term potentiation and memory stability (Karlsson et al., 2016; Schwab and Strittmatter, 2014). However, it is not known whether Nogo-A-evoked cellular responses are modulated by HSPGs.

In this study, we identified HSPGs as novel functional receptors for the active Nogo-A domain Nogo-A-Δ20 (rat amino acid (aa) 544-725 (Oertle et al., 2003)). We found that Nogo-A-Δ20 activates RhoA and inhibits cell spreading and neurite outgrowth via HSPGs, specifically via the transmembrane HSPGs syndecan-4 and syndecan-3. In addition, we show that Nogo-A-Δ20 inhibits cell adhesion of neuroblasts in an HSPG-dependent manner and increases neuroblast chain migration ex vivo. Our results propose a novel mechanism by which Nogo-A-Δ20 affects cytoskeletal dynamics by interacting with HSPGs independently of the newly characterized Nogo-A-Δ20 receptor Sphingosine-1-Phosphate receptor 2 (S1PR2) (Kempf et al., 2014).

Results

Cell surface heparan sulfate is required for Nogo-A-Δ20-induced inhibition of cell spreading

Outgrowth of neurites and spreading of cells, e.g. fibroblasts, are strongly inhibited by substrates containing Nogo-A or its active fragment Nogo-A-Δ20 (Oertle et al., 2003) (Figure 1A). To determine a possible role of heparan sulfate (HS), cell spreading inhibition was examined upon enzymatic cleavage of HS. Treatment of Swiss 3T3 cells with heparinase III (HepIII) significantly increased cell spreading by ~45% on the Nogo-A-Δ20-coated culture dishes when compared to the vehicle (saline) control (Figure 1A,B). Treatment with heparinase I (HepI), which cleaves HS at the level of *O*-sulfated rather than non-sulfated or *N*-sulfated disaccharides (Hovingh and Linker, 1970), resulted in a similar decrease of the Nogo-A-Δ20 inhibition but required higher enzyme concentrations (Figure S1A).

If endogenous HS promotes the Nogo-A-Δ20 inhibitory effects by directly binding to Nogo-A, excess soluble HS in the culture medium may act as competitive inhibitor and neutralize Nogo-A-mediated cell spreading inhibition. Indeed, acute application of exogenous HS significantly increased cell spreading on a Nogo-A-Δ20 substrate when compared to control treatment (Figure 1A,C). Similar effects were also observed when HS was added onto Nogo-A-Δ20-coated plates and washed prior to the plating of the cells, suggesting that Nogo-A-Δ20-bound HS neutralizes cell spreading inhibition (Figure S1B).

To confirm the involvement of HS in Nogo-A-Δ20 signaling, a HS-deficient mutant CHO cell line, pgsD-677 (Lidholt et al., 1992), was examined. Due to a mutation in the *Ext1* gene encoding for a glycosyltransferase responsible for HS polymerization, pgsD-677 cells do not produce HS (Lidholt et al., 1992). Whereas wild type CHO cells were strongly inhibited in spreading by Nogo-A-Δ20, spreading inhibition was almost fully abolished in the HSPG-deficient pgsD-677 cells (Figure 1D,E). To confirm that these results are effectively due to the

lack of HS, we analysed cell spreading upon re-expression of *Ext1* in pgsD-677 cells. Indeed, *Ext1* re-expression fully restored Nogo-A-Δ20-mediated cell spreading inhibition (Figure 1D,F). The flow cytometry analysis of cell surface HSPGs expression confirmed their absence in pgsD-677 cells, as well as their partial reduction after HepIII treatment and their restoration after *Ext1* re-expression (Figure 1G).

Cell surface heparan sulfate is required for Nogo-A-Δ20-induced inhibition of neurite outgrowth

We examined the functional role of HS in Nogo-A-Δ20-mediated inhibition of neurite outgrowth using postnatal day (P) 5-8 mouse cerebellar granule neurons (CGNs) as a model system. Notably, CGNs would not adhere if HepIII was applied acutely. Instead, HepIII was applied 12 h after plating for a total duration of 24 h. Delayed treatment of CGNs with HepIII fully abolished the growth-inhibitory effect of Nogo-A-Δ20: neurite outgrowth was increased by ~92% when compared to the saline control (Figure 2A,B).

To extend these findings to other neuronal populations, we analysed the effect of HepIII treatment in postnatal dorsal root ganglion (DRG) neurons and embryonic (E19) cortical neurons. Similar to CGNs, HepIII treatment fully abolished Nogo-A-Δ20-induced inhibition of neurite outgrowth in DRG (Figure 2C,D) and cortical neurons (Figure 2E,F). Together, these results provide strong evidence for the requirement of HS chains on the surface of Nogo-A responsive cells to promote Nogo-A-Δ20-mediated inhibition of neurite outgrowth.

Nogo-A-Δ20 binds heparan sulfate and brain-derived glycosaminoglycans

To investigate a possible direct binding of Nogo-A-Δ20 to HS, we used an ELISA assay. Biotinylated preparations of HS and heparin, a highly sulfated form of HS (Bernfield et al., 1999), were immobilized and tested for T7-tagged Nogo-A-Δ20 binding using two different antibodies: an anti-T7 tag and a Nogo-A-specific antibody targeting the Δ20 domain (11c7 (Oertle et al., 2003)). To assess the binding specificity of Nogo-A-Δ20 to HS, three different

variants of chondroitin sulfate (CS), another form of glycosaminoglycans (GAGs), were tested in parallel (CS-A, CS-C and CS-E). In addition, another inhibitory domain of Nogo-A, Nogo-66 (rat aa 1026-1091), which is known to interact with a different receptor complex (Kempf and Schwab, 2013), was tested. Importantly, Nogo-66 inhibits neurite outgrowth but not cell spreading (Kempf and Schwab, 2013). Recombinant Nogo-66-Fc was detected using an Fc-specific antibody. Nogo-A-Δ20 but not Nogo-66 showed very strong binding to HS and to heparin and significantly less to CS-A, CS-C or CS-E ($p < 0.001$) (Figure 3A). These results were replicated using GAGs extracted from adult rat brains (total GAGs) treated with HepI/III or ChondroitinaseABC (ChABC) to obtain CS-containing GAGs (CS-GAGs) or HS-containing GAGs (HS-GAGs), respectively. Consistent with the above results, Nogo-A-Δ20 bound total GAGs and HS-GAGs very strongly and showed significantly less binding to CS-GAGs ($p < 0.001$) (Figure 3B). No binding of Nogo-66 to total GAGs, HS-GAGs or CS-GAGs was observed (Figure 3B). In order to determine the specificity of the binding of Nogo-A-Δ20 to CS-GAGs, we tested the binding of the control protein Nogo-A-Δ21 (rat aa 812-918) (Oertle et al., 2003), which lacks inhibitory activity but is purified under identical conditions, to brain-derived GAGs. No difference in binding was observed between Nogo-A-Δ21, total GAGs, HS-GAGs or CS-GAGs (Figure S2). Moreover, the absorbance values lie in the same range than those of Nogo-A-Δ20 binding to CS-GAGs, suggesting than the binding of Nogo-A-Δ20 to CS-GAGs is likely to be unspecific. Given the fact that the results in Figure 3B, 3D and S2A are standardised against the total GAGs and that the HS:CS ratio in the brain is 1:10 (Deepa et al., 2006), Nogo-A-Δ20 shows a strong binding preference to HS-GAGs. Together, these results indicate that the key and main binding partner of Nogo-A-Δ20 is HS.

Finally, to determine the binding affinity of Nogo-A-Δ20 to heparin or HS-GAGs, a dose-response binding curve was measured (Figure 3C,D). Binding was saturable and non-linear

158 fitting revealed that Nogo-A-Δ20 binds to heparin and HS-GAGs with a dissociation constant
159 (K_d) of ~234 nM and ~562 nM, respectively (Figure 3C, D).
160 To assess the ability of Nogo-A-Δ20 to bind HS under physiological conditions, cell surface
161 binding assays were performed in CHO WT and pgsD-677 cells. Cells were incubated with
162 HA-tagged Nogo-A-Δ20 for 1 h at 4°C, washed and immunostained for the HA tag (Figure
163 3E). Nogo-A-Δ20 binding was assessed by measuring the number of Nogo-A-Δ20 puncta per
164 cell surface area calculated upon 3D reconstruction of the cells. High numbers of Nogo-A-
165 Δ20 puncta per WT CHO cell were found, whereas no binding of Nogo-A-Δ20 was detected
166 in CHO pgs-D677 cells (Figure 3F). Similar results were also obtained in 3T3 cells after
167 HepIII treatment (Figure 3G) showing that Nogo-A-Δ20 binds HSPGs.
168 **Nogo-A-Δ20 acts via HSPGs independently of S1PR2**
169 Cell surface HSPGs can act as co-receptors by promoting the binding of a ligand to its
170 obligate receptor and thereby altering its activation (Bernfield et al., 1999; Sarrazin et al.,
171 2011). Given the prior identification of the G-protein-coupled receptor (GPCR) Sphingosine-
172 1-Phosphate receptor 2 (S1PR2) as a functional receptor for Nogo-A-Δ20 (Kempf et al.,
173 2014), HSPGs may enhance or allow the formation of a Nogo-A-Δ20/S1PR2 complex.
174 Alternatively, HSPGs may transduce Nogo-A-Δ20 signals independently of S1PR2. In the
175 latter case, we reasoned that HepIII treatment of S1PR2-deficient cells should show a
176 disinhibition effect; in the former case, no effect of HepIII should be observed given the
177 requirement of S1PR2 as obligate receptor. To test this, $S1PR2^{-/-}$ mouse embryonic fibroblasts
178 (MEFs) (Kempf et al., 2014) were treated with HepIII or saline and plated on Nogo-A-Δ20
179 (Figure 4A, S3A). Strikingly, treatment of $S1PR2^{-/-}$ MEFs with HepIII significantly further
180 increased cell spreading on Nogo-A-Δ20 when compared to HepIII-treated WT MEFs or
181 $S1PR2^{-/-}$ MEFs alone (Figure 4A, S3A). This suggests that Nogo-A-Δ20 can act via HSPGs
182 independently of S1PR2.

In CHO-K1 WT cells, the levels of endogenous S1PRs mRNAs were shown to be below detection limit, and these cells were unresponsive to the S1PR family ligand S1P in a variety of *in vitro* assays (e.g., (Gonda et al., 1999; Okamoto et al., 1998)). Based on these observations, CHO-K1 WT cells are considered as devoid of S1PR expression. To validate this under our experimental conditions, CHO WT cells were treated with the pharmacological S1PR2 antagonist JTE-013 and plated onto Nogo-A-Δ20 and control substrates (Figure 4B, S3B). As expected, JTE-013 did not antagonize Nogo-A-Δ20-dependent inhibition of cell spreading (Figure 4B, S3B). The same observation was made in mutant pgsD-677 cells (Figure 4B, S3B). Together, these results suggest that Nogo-A-Δ20 can exert inhibitory effects via HSPGs in S1PR2-deficient cellular systems.

Nogo-A-Δ20 has been repeatedly shown to activate the RhoA/ROCK pathway and thereby to inhibit cell spreading and neurite outgrowth (Kempf et al., 2014; Niederost et al., 2002). To test whether HSPGs can also mediate Nogo-A-Δ20-induced downstream signaling, RhoA activation was measured in CHO WT and pgsD-677 cells. In CHO WT cells, a ~250% increase in RhoA activation was observed 20 min after application of Nogo-A-Δ20, whereas no change was observed in pgsD-677 cells (Figure 4C,D). The inactive Nogo-A fragment Nogo-A-Δ21 was used as control protein. Further, no change in RhoA activation was observed in the presence of JTE-013 (Figure S4A) suggesting the presence of an S1PR2-independent, HSPG-dependent Nogo-A-Δ20 signal transduction pathway.

To determine whether Nogo-A-Δ20 inhibition in CHO WT cells could be overcome by blocking RhoA or the downstream Rho-associated kinase (ROCK), CHO WT cell were treated with the RhoA inhibitor C3 transferase or with the ROCK inhibitor Y-27632 and plated onto Nogo-A-Δ20 (Figure 4E,F). In line with the RhoA activation results, blockade of RhoA or ROCK showed a full rescue of Nogo-A-Δ20 inhibition (Figure 4E,F).

Finally, in order to determine the effect of simultaneous blockade of HSPGs and S1PR2 in cells co-expressing HSPGs and S1PR2, 3T3 cells were treated with HepIII and/or JTE-013 and assessed in a cell spreading assay. Strikingly, blockade of HSPGs and S1PR2 showed an additive effect in reducing Nogo-A-Δ20 induced inhibition of cell spreading (Figure S3C,D). Hence, in cells co-expressing both receptors, Nogo-A-Δ20 can exert inhibitory effects via both S1PR2 as well as HSPGs. However, as shown by using S1PR2-deficient cells, HSPGs are themselves sufficient to mediate Nogo-A-Δ20 inhibition and RhoA activation.

Syndecans mediate Nogo-A-Δ20 inhibition of cell spreading and neurite outgrowth

Membrane-bound cell surface HSPGs consist of two main families: syndecans and glypicans (Bernfield et al., 1999). As opposed to syndecans, glypicans are attached by a glycosylphosphatidylinositol anchor to the membrane and do not exert cytoplasmic signaling roles (Bernfield et al., 1999). The syndecan family consists of four members: syndecan-1 to syndecan-4 (Sdc1-Sdc4) (Bernfield et al., 1999), of which syndecan-4 is the most highly expressed in 3T3 cells (Figure 5A). Interestingly, syndecan-4 has been shown to activate RhoA to promote focal adhesion maturation and stress fibre assembly following engagement with fibronectin (Brooks 2012, Dovas 2006).

To test the contribution of syndecan-4 to Nogo-A-Δ20-induced inhibition of cell spreading and RhoA activation, syndecan-4 was knocked down using lentivirus-delivered ctrl and syndecan-4 shRNA (Figure S5A). Strikingly, knockdown of syndecan-4 fully prevented Nogo-A-Δ20 inhibition of cell spreading (Figure 5B,C). To test whether Nogo-A-Δ20 activates RhoA via syndecan-4, RhoA activation assays were performed in ctrl vs syndecan-4 shRNA cells. The inactive Nogo-A fragment Nogo-A-Δ21 was used as control protein. No RhoA activation was observed upon syndecan-4 knockdown (Figure 5G). Together, these results suggest that Nogo-A-Δ20 inhibits cell spreading by activating RhoA via syndecan-4 in fibroblasts.

To investigate whether syndecans are also important in Nogo-A-Δ20-induced inhibition of neurite outgrowth, we first assessed their expression in DIV4 E19 rat cortical neurons and found syndecan-3 to be the most highly expressed (Figure 5D). Remarkably, siRNA-mediated knockdown of syndecan-3 fully prevented outgrowth inhibition on the Nogo-A-Δ20 substrate (Figure 5E,F; S5B).

Further, to test whether syndecan-3 and syndecan-4 directly interact with Nogo-A-Δ20, microscale thermophoresis binding experiments were performed using recombinant syndecan-3 and syndecan-4 ectodomains. We found that Nogo-A-Δ20 binds to syndecan-4 and syndecan-3 in a similar affinity range than to brain-derived HS-GAGs with a K_d of ~522.1 nM and ~865.7 nM, respectively (Figure 5H). Taken together, these data show that Nogo-A-Δ20 binds to and exerts inhibitory effects via syndecan-3 or -4 in a cell type-specific manner.

Nogo-A-Δ20 promotes neuroblast migration via HSPGs

Nogo-A-Δ20 was shown to promote the tangential migration of neuroblasts from the subventricular zone (SVZ) to the olfactory bulb along the rostral migratory stream (RMS) through activation of the Rho/ROCK pathway (Rolando et al., 2012). Yet, no molecular basis for this observation was found and we sought to determine the physiological relevance of the Nogo-A-Δ20/HSPG interaction in this process.

To investigate the contribution of HSPGs to SVZ-derived neuroblast migration, postnatal explants of the SVZ and RMS were used as an ex vivo model (Wichterle et al., 1997) and treated with HepIII and/or the Nogo-A-Δ20 function-blocking antibody 11c7. In this assay, neuroblasts move out of the explant core by chain migration (i.e. associated with each other) as occurs in the RMS in vivo (Wichterle et al., 1997). As previously shown, Nogo-A neutralization by 11c7 induced a significant reduction of the migration area (Figure 6A,B). HepIII treatment induced a similar reduction of the migration (Figure 6A,B). To examine whether HSPGs and Nogo-A-Δ20 operate through the same pathway, we co-administered

HepIII and 11c7. Co-application of HepIII and 11c7 led to a reduction in migration area similar to that obtained upon treatment of HepIII or 11c7 alone (Figure 6A,B) suggesting that Nogo-A-Δ20 operates through HSPGs in this system.

Previous data suggested that Nogo-A sustains neuroblast migration by providing anti-adhesive signals (Rolando et al., 2012). To investigate whether HSPGs participate in Nogo-A-Δ20-mediated repulsive effects, we asked whether HepIII treatment affected neuroblast adhesion on control vs. Nogo-A-Δ20-coated substrates in the presence or absence of 11c7. HepIII treatment significantly increased cell adhesion on Nogo-A-Δ20 to a similar extent than 11c7 (Figure 6C). No additive or synergistic effects were observed (Figure 6C), suggesting that Nogo-A-Δ20 and HSPGs share a common pathway in ex vivo cultures.

Finally, to test the role of the previously identified Nogo-A-Δ20 receptor S1PR2 in neuroblast migration, explants were treated with the S1PR2 blocker JTE-013 or DMSO (vehicle control). No significant effect on the migration area was observed using different concentrations of JTE-013 (Figure 6D,E). Similarly, JTE-013 treatment had no effect on neuroblast adhesion (Figure 6F). Taken together, these data show that Nogo-A-Δ20 inhibits adhesion and increases migration by providing anti-adhesive signals through HSPGs but not S1PR2.

Discussion

Cell-to-cell signaling by ligand receptor interactions as well as interactions with ECM constituents play key roles during developmental processes such as neuronal migration and axon growth. In this study, we identify a novel biochemical interaction between the membrane protein Nogo-A and HSPGs and demonstrate its functional significance in cell spreading, neurite outgrowth, adhesion and neuroblast chain migration.

Cell surface HSPGs are traditionally viewed as co-receptors that promote the binding of a ligand to its obligate receptor through their large glycosaminoglycan chains (Bernfield et al., 1999; Sarrazin et al., 2011) but do not act as signal-transducing receptors themselves. In the case of FGF and many other morphogens, HS is essential for the ligand/receptor complex to form and to alter its activation (Sarrazin et al., 2011). Surprisingly, our data suggest that this is not the case for Nogo-A-Δ20 and its S1PR2 receptor (Kempf et al., 2014): Nogo-A-Δ20 can activate RhoA in S1PR-negative CHO cells and inhibits cell spreading in $S1PR2^{-/-}$ MEFs. Hence, our results strongly suggest that Nogo-A-Δ20 can signal through S1PR-independent mechanisms. However, when HSPGs and S1PR2 are co-expressed, both pathways can act in parallel, as shown for fibroblasts, or one pathway can gain control of the signaling output, as demonstrated for neuroblasts. Collectively, our experiments reveal that more than one receptor for the active Nogo-A-Δ20 region exists and that Nogo-A-Δ20-induced inhibitory effects are regulated in a cell type-specific manner.

Based on our findings showing the involvement of syndecan-3 and syndecan-4, we may hypothesize that the cytoplasmic tail of syndecans is important for Nogo-A-Δ20-induced signal transduction upon extracellular binding to the HS chains. A few studies have shown that transmembrane syndecans can act as signaling receptors through their cytoplasmic

299 domains. During cell migration, engagement of syndecan-4 by fibronectin was shown to
300 result in the activation of protein kinase C α (PKCα) upstream of RhoA activation (Bass et
301 al., 2008; Bass et al., 2007; Brooks et al., 2012; Dovas et al., 2006). Even though it is unclear
302 how syndecan-4 signals to RhoA via PKCα, PKCα was shown to activate RhoA via
303 phosphorylation of the Rho guanine exchange factor (RhoGEF) p115 in a different system
304 (Peng et al 2011). It will be interesting to investigate whether Nogo-A-Δ20 operates via
305 similar mechanisms. In the case of syndecan-3, binding of the heparin-binding growth-
306 associated molecule HB-GAM was shown to result in phosphorylation of the Src kinases c-
307 Src and c-Fyn, and of cortactin, which promotes polymerization and rearrangement of the
308 actin cytoskeleton resulting in neurite outgrowth (Kinnunen et al., 1998). A similar
309 mechanism was proposed for glial cell line-derived neurotrophic factor (GDNF) family
310 ligands and syndecan-3 (Bespalov et al., 2011). However, no link between syndecan-3 and
311 RhoA activation has been reported so far and future studies shall address this point.
312
313 Syndecan-3 is the major HSPG found in neurons of the developing brain and shows abundant
314 expression in major axonal tracts and migratory routes, e.g., in the RMS (Hienola et al., 2006;
315 Nolo et al., 1995; Rauvala et al., 2000). In the adult brain, syndecan-3 is strongly expressed in
316 the hippocampus, cerebellum and cortex and in several axonal tracts (Hsueh and Sheng,
317 1999). Our results show that the anti-adhesive effect of Nogo-A-Δ20 is accompanied by an
318 HS-dependent increase in neuroblast chain migration. Notably, syndecan-$3^{-/-}$ mice phenocopy
319 the defects in radial and tangential neuronal migration observed in Nogo-$A^{-/-}$ mice (Hienola et
320 al., 2006; Mathis et al., 2010; Mingorance-Le Meur et al., 2007; Rolando et al., 2012).
321 Syndecan-$3^{-/-}$ mice also display a synaptic plasticity phenotype similar to that observed in
322 Nogo-$A^{-/-}$ mice: increased CA1 long-term potentiation (LTP) while baseline transmission and
323 short-term plasticity are not affected (Kaksonen et al., 2002). Given the recent implication of

HSPGs in synapse formation and plasticity (Allen et al., 2012; de Wit et al., 2013; Siddiqui et al., 2013), it will be interesting to determine whether Nogo-A also mediates its effects on synapse formation and plasticity via HSPGs (Mironova and Giger, 2013). Overall, the localization of syndecan proteins and their physiological impact in the developing and adult brain are consistent with a functional interaction between Nogo-A and HSPGs *in vivo*.

In conclusion, our study shows that Nogo-A-Δ20 can regulate adhesion, cell spreading, outgrowth and migration of various cell lines, neurons and neuroblasts via a newly identified interaction with transmembrane HSPGs.

Experimental procedures

Plasmids, recombinant fusion proteins, reagents, antibodies and brain-derived glycosaminoglycans (GAGs)

A complete description is provided in the Supplemental Experimental Procedures.

Tissue preparation and cell culture

A complete description is provided in the Supplemental Experimental Procedures.

Immunocytochemistry, flow cytometry and RhoA activation assays

Immunocytochemistry, cell surface binding assays, flow cytometry and RhoA pulldown/ELISA experiments were essentially performed as previously described (Kempf et al., 2014). A complete description is provided in the Supplemental Experimental Procedures.

In vitro bioassays

3T3 fibroblast spreading assays and neurite outgrowth assays were performed as described previously (Kempf et al., 2014; Oertle et al., 2003). For HepI and HepIII (Sigma) treatment, cells were incubated with 2.5-10 U/ml HepI or HepIII 3 h prior plating and during the spreading assay. For function-blocking experiments, cells were incubated with 1 μM JTE-013, 5 μM Y-27632 or 100 μg/ml C3 30 min prior plating and during the spreading assay. The corresponding solvents were used as controls. For expression of EXT1 in pgsD-677 cells, pgsD-677 cells were transfected with Ext1 cDNA using Lipofectamine 2000 (Invitrogen) according to the manufacturer's instructions. For siRNA experiments, 3T3 cells or E19 rat cortical neurons were transfected with ON-TARGETplus SMARTpool siRNAs using DharmaFECT3 (Dharmacon) according to the manufacturer's instructions. For shRNA experiments, stable 3T3 shRNA cell lines were made using lentiviruses carrying Mission shRNA pLKO lentiviral plasmids (Sigma) containing shRNA against Sdc4 or ctrl shRNA. A complete description is provided in the Supplemental Experimental Procedures.

ELISA

The ELISA was performed according to method described in (Purushothaman et al., 2007) with modifications detailed in Supplemental Experimental Procedures.

Explant assay

P5 explants were prepared from C57/BL6 pups according to (Wichterle et al., 1997) with modifications detailed in Supplemental Experimental Procedures.

Statistical analysis

Statistical analyses were conducted using the statistical software GraphPad Prism 5 or 6 (GraphPad Software Inc.). $*p < 0.05$ was considered statistically significant. Calculations were corrected for multiple comparisons as specified.

Author contributions

A.K. and M.E.S. designed the research and wrote the paper; A.K. performed most biochemical and cellular experiments and analyzed data. Z.R. performed flow cytometry experiments. A.M.K., Z.R., A.S., A.S. and B.T. performed some bioassays. J.C.F.K. and J.W.F. performed GAG ELISA experiments and analyzed data. V.G., E.B. and A.B. performed neuroblast migration and adhesion experiments and analyzed data.

Acknowledgements

We thank H. Rauvala for helpful discussions and J. Esko for providing *Ext1* cDNA. This work was supported by the Swiss National Science Foundation (grants 3100A0-122527/1 and 310030B- 138676/1), the ERC advanced grant 294115 'Nogorise' and the National Centre for Competence in Research "Neural Plasticity and Repair" of the Swiss National Science Foundation.

References

Allen, N.J., Bennett, M.L., Foo, L.C., Wang, G.X., Chakraborty, C., Smith, S.J., and Barres, B.A. (2012). Astrocyte glypicans 4 and 6 promote formation of excitatory synapses via GluA1 AMPA receptors. Nature *486*, 410-414.

Bass, M.D., Morgan, M.R., Roach, K.A., Settleman, J., Goryachev, A.B., and Humphries, M.J. (2008). p190RhoGAP is the convergence point of adhesion signals from alpha 5 beta 1 integrin and syndecan-4. J Cell Biol *181*, 1013-1026.

Bass, M.D., Roach, K.A., Morgan, M.R., Mostafavi-Pour, Z., Schoen, T., Muramatsu, T., Mayer, U., Ballestrem, C., Spatz, J.P., and Humphries, M.J. (2007). Syndecan-4-dependent Rac1 regulation determines directional migration in response to the extracellular matrix. J Cell Biol *177*, 527-538.

Bernfield, M., Gotte, M., Park, P.W., Reizes, O., Fitzgerald, M.L., Lincecum, J., and Zako, M. (1999). Functions of cell surface heparan sulfate proteoglycans. Annu Rev Biochem *68*, 729-777.

Bespalov, M.M., Sidorova, Y.A., Tumova, S., Ahonen-Bishopp, A., Magalhaes, A.C., Kulesskiy, E., Paveliev, M., Rivera, C., Rauvala, H., and Saarma, M. (2011). Heparan sulfate proteoglycan syndecan-3 is a novel receptor for GDNF, neurturin, and artemin. J Cell Biol *192*, 153-169.

Brooks, R., Williamson, R., and Bass, M. (2012). Syndecan-4 independently regulates multiple small GTPases to promote fibroblast migration during wound healing. Small GTPases *3*, 73-79.

de Wit, J., O'Sullivan, M.L., Savas, J.N., Condomitti, G., Caccese, M.C., Vennekens, K.M., Yates, J.R., 3rd, and Ghosh, A. (2013). Unbiased discovery of glypican as a receptor for LRRTM4 in regulating excitatory synapse development. Neuron *79*, 696-711.

Deepa, S.S., Carulli, D., Galtrey, C., Rhodes, K., Fukuda, J., Mikami, T., Sugahara, K., and Fawcett, J.W. (2006). Composition of perineuronal net extracellular matrix in rat brain: a different disaccharide composition for the net-associated proteoglycans. J Biol Chem *281*, 17789-17800.

Dovas, A., Yoneda, A., and Couchman, J.R. (2006). PKCbeta-dependent activation of RhoA by syndecan-4 during focal adhesion formation. J Cell Sci *119*, 2837-2846.

Gonda, K., Okamoto, H., Takuwa, N., Yatomi, Y., Okazaki, H., Sakurai, T., Kimura, S., Sillard, R., Harii, K., and Takuwa, Y. (1999). The novel sphingosine 1-phosphate receptor AGR16 is coupled via pertussis toxin-sensitive and -insensitive G-proteins to multiple signaling pathways. Biochem J *337 (Pt 1)*, 67-75.

Hienola, A., Tumova, S., Kulesskiy, E., and Rauvala, H. (2006). N-syndecan deficiency impairs neural migration in brain. J Cell Biol *174*, 569-580.

Hovingh, P., and Linker, A. (1970). The enzymatic degradation of heparin and heparitin sulfate. 3. Purification of a heparitinase and a heparinase from flavobacteria. J Biol Chem *245*, 6170-6175.

Hsueh, Y.P., and Sheng, M. (1999). Regulated expression and subcellular localization of syndecan heparan sulfate proteoglycans and the syndecan-binding protein CASK/LIN-2 during rat brain development. J Neurosci *19*, 7415-7425.

Hu, H. (2001). Cell-surface heparan sulfate is involved in the repulsive guidance activities of Slit2 protein. Nat Neurosci *4*, 695-701.

Inatani, M., Irie, F., Plump, A.S., Tessier-Lavigne, M., and Yamaguchi, Y. (2003). Mammalian brain morphogenesis and midline axon guidance require heparan sulfate. Science *302*, 1044-1046.

Irie, F., Okuno, M., Matsumoto, K., Pasquale, E.B., and Yamaguchi, Y. (2008). Heparan sulfate regulates ephrin-A3/EphA receptor signaling. Proc Natl Acad Sci U S A *105*, 12307-12312.

Kaksonen, M., Pavlov, I., Voikar, V., Lauri, S.E., Hienola, A., Riekki, R., Lakso, M., Taira, T., and Rauvala, H. (2002). Syndecan-3-deficient mice exhibit enhanced LTP and impaired hippocampus-dependent memory. Mol Cell Neurosci *21*, 158-172.

Karlsson, T.E., Smedfors, G., Brodin, A.T., Aberg, E., Mattsson, A., Hogbeck, I., Wellfelt, K., Josephson, A., Brene, S., and Olson, L. (2016). NgR1: A Tunable Sensor Regulating Memory Formation, Synaptic, and Dendritic Plasticity. Cereb Cortex *26*, 1804-1817.

Kempf, A., and Schwab, M.E. (2013). Nogo-A represses anatomical and synaptic plasticity in the central nervous system. Physiology *28*, 151-163.

Kempf, A., Tews, B., Arzt, M.E., Weinmann, O., Obermair, F.J., Pernet, V., Zagrebelsky, M., Delekate, A., Iobbi, C., Zemmar, A.*, et al.* (2014). The sphingolipid receptor S1PR2 is a receptor for Nogo-a repressing synaptic plasticity. PLoS Biol *12*, e1001763.

Kinnunen, T., Kaksonen, M., Saarinen, J., Kalkkinen, N., Peng, H.B., and Rauvala, H. (1998). Cortactin-Src kinase signaling pathway is involved in N-syndecan-dependent neurite outgrowth. J Biol Chem *273*, 10702-10708.

Lidholt, K., Weinke, J.L., Kiser, C.S., Lugemwa, F.N., Bame, K.J., Cheifetz, S., Massague, J., Lindahl, U., and Esko, J.D. (1992). A single mutation affects both N-acetylglucosaminyltransferase and glucuronosyltransferase activities in a Chinese hamster ovary cell mutant defective in heparan sulfate biosynthesis. Proc Natl Acad Sci U S A *89*, 2267-2271.

Mathis, C., Schroter, A., Thallmair, M., and Schwab, M.E. (2010). Nogo-a regulates neural precursor migration in the embryonic mouse cortex. Cereb Cortex *20*, 2380-2390.

Mingorance-Le Meur, A., Zheng, B., Soriano, E., and del Rio, J.A. (2007). Involvement of the myelin-associated inhibitor Nogo-A in early cortical development and neuronal maturation. Cereb Cortex *17*, 2375-2386.

Mironova, Y.A., and Giger, R.J. (2013). Where no synapses go: gatekeepers of circuit remodeling and synaptic strength. Trends Neurosci *36*, 363-373.

Niederost, B., Oertle, T., Fritsche, J., McKinney, R.A., and Bandtlow, C.E. (2002). Nogo-A and myelin-associated glycoprotein mediate neurite growth inhibition by antagonistic regulation of RhoA and Rac1. The Journal of neuroscience *22*, 10368-10376.

Nolo, R., Kaksonen, M., Raulo, E., and Rauvala, H. (1995). Co-expression of heparin-binding growth-associated molecule (HB-GAM) and N-syndecan (syndecan-3) in developing rat brain. Neurosci Lett *191*, 39-42.

Oertle, T., van der Haar, M.E., Bandtlow, C.E., Robeva, A., Burfeind, P., Buss, A., Huber, A.B., Simonen, M., Schnell, L., Brosamle, C*., et al.* (2003). Nogo-A inhibits neurite outgrowth and cell spreading with three discrete regions. The Journal of neuroscience *23*, 5393-5406.

Okamoto, H., Takuwa, N., Gonda, K., Okazaki, H., Chang, K., Yatomi, Y., Shigematsu, H., and Takuwa, Y. (1998). EDG1 is a functional sphingosine-1-phosphate receptor that is linked via a Gi/o to multiple signaling pathways, including phospholipase C activation, Ca2+ mobilization, Ras-mitogen-activated protein kinase activation, and adenylate cyclase inhibition. J Biol Chem *273*, 27104-27110.

Purushothaman, A., Fukuda, J., Mizumoto, S., ten Dam, G.B., van Kuppevelt, T.H., Kitagawa, H., Mikami, T., and Sugahara, K. (2007). Functions of chondroitin sulfate/dermatan sulfate chains in brain development. Critical roles of E and iE disaccharide units recognized by a single chain antibody GD3G7. J Biol Chem *282*, 19442-19452.

Rauvala, H., Huttunen, H.J., Fages, C., Kaksonen, M., Kinnunen, T., Imai, S., Raulo, E., and Kilpelainen, I. (2000). Heparin-binding proteins HB-GAM (pleiotrophin) and amphoterin in the regulation of cell motility. Matrix Biol *19*, 377-387.

Rolando, C., Parolisi, R., Boda, E., Schwab, M.E., Rossi, F., and Buffo, A. (2012). Distinct roles of nogo-a and nogo receptor 1 in the homeostatic regulation of adult neural stem cell function and neuroblast migration. J Neurosci *32*, 17788-17799.

Sarrazin, S., Lamanna, W.C., and Esko, J.D. (2011). Heparan sulfate proteoglycans. Cold Spring Harb Perspect Biol *3*.

Schwab, M.E. (2010). Functions of Nogo proteins and their receptors in the nervous system. Nat Rev Neurosci *11*, 799-811.

Schwab, M.E., and Strittmatter, S.M. (2014). Nogo limits neural plasticity and recovery from injury. Curr Opin Neurobiol *27*, 53-60.

Siddiqui, T.J., Tari, P.K., Connor, S.A., Zhang, P., Dobie, F.A., She, K., Kawabe, H., Wang, Y.T., Brose, N., and Craig, A.M. (2013). An LRRTM4-HSPG complex mediates excitatory synapse development on dentate gyrus granule cells. Neuron *79*, 680-695.

Strochlic, L., Dwivedy, A., van Horck, F.P., Falk, J., and Holt, C.E. (2008). A role for S1P signaling in axon guidance in the Xenopus visual system. Development *135*, 333-342.

Van Vactor, D., Wall, D.P., and Johnson, K.G. (2006). Heparan sulfate proteoglycans and the emergence of neuronal connectivity. Curr Opin Neurobiol *16*, 40-51.

Wichterle, H., Garcia-Verdugo, J.M., and Alvarez-Buylla, A. (1997). Direct evidence for homotypic, glia-independent neuronal migration. Neuron *18*, 779-791.

Yamaguchi, Y. (2001). Heparan sulfate proteoglycans in the nervous system: their diverse roles in neurogenesis, axon guidance, and synaptogenesis. Semin Cell Dev Biol *12*, 99-106.

Figure legends

Figure 1. Cell surface HSPGs mediate Nogo-A-Δ20 inhibition of cell spreading. A. Representative pictures of 3T3 fibroblasts treated with 2.5 U/ml HepIII, 0.1 mg/ml HS or vehicle (saline) and plated on control (ctrl) or Nogo-A-Δ20 substrate. Cells were stained with Phalloidin-Alexa488. **B,C.** Cell spreading quantification of **A**. HepIII (**B**) or HS (**C**) treatment partially reversed Nogo-A-Δ20-mediated cell spreading inhibition. **D.** Representative pictures of CHO WT, CHO pgsD-677 or CHO pgsD-677 expressing *Ext1* cDNA and plated on a control or Nogo-A-Δ20 substrate. **E,F.** Cell spreading quantification of **D**. **E.** The rounding response to Nogo-A-Δ20 is highly impaired in CHO pgsD-677 mutants. **F.** Expression of EXT1 in CHO pgsD-677 cells fully restored Nogo-A-Δ20 inhibition. **G.** Flow cytometry detection of cell surface HSPGs in 3T3 cells (upper panel) or CHO WT and pgsD-677 cells (lower panel) using the 10E4 antibody. HepIII treatment of 3T3 cells reduces HSPG levels. EXT1 expression restores HSPG levels in CHO pgsD-677 cells. WT designates CHO cells. Filled grey curves indicate unstained controls. The fluorescence intensity is displayed on the X-axis (256 bins) and the normalized number of cells per each bin on the Y-axis. Data shown are means ± SEM (n = 8-12 coverslips). **B,C,E,F**: One-way ANOVA with Tuckey's post hoc test; (*** $p < 0.001$). Scale bars: 45 μm. See also Figure S1.

Figure 2. Cell surface HSPGs mediate Nogo-A-Δ20 inhibition of neurite outgrowth. A. Representative pictures of mouse P7 cerebellar granule neurons (CGNs) treated with 500 mU/ml HepIII or vehicle (saline) and plated on a control (ctrl) or Nogo-A-Δ20 substrate. Neurons were stained with βIII-Tubulin. **B.** Total neurite length per cell quantification of **A**. HepIII treatment fully reversed Nogo-A-Δ20-mediated inhibition of neurite outgrowth. **C.** Representative pictures of mouse P7 dorsal root ganglia (DRG) neurons treated with 1 U/ml HepIII or vehicle (saline) and plated on a control or Nogo-A-Δ20 substrate. Neurons were

stained with βIII-Tubulin. **D.** Total neurite length per cell quantification of **C**. **E.** Representative pictures of DIV5 rat E19 cortical neurons treated with 1 U/ml HepIII or vehicle (saline) at DIV4 and replated on a control (ctrl) or Nogo-A-Δ20 substrate for 24h. Neurons were stained with Map1b. **F.** Total neurite length per cell quantification of **E**. DIV, days in vitro. Data shown are means ± SEM (n = 3-9 coverslips). **B,D,F**: One-way ANOVA with Tuckey's post hoc test; (* $p < 0.05$, *** $p < 0.001$; ns: not significant). Scale bars: 45 μm.

Figure 3. Nogo-A-Δ20 but not Nogo-66 binds Heparin and HS. A-D. Biotinylated heparin, HS, CS or brain-derived GAGs were coated onto streptavidin-coated wells and analysed for Nogo-A-Δ20 or Nogo-66 binding by an ELISA-type assay. Average values for the BSA negative control were subtracted from the respective readings. Nogo-A-Δ20-T7 binding was detected using an anti-T7 or anti-Nogo-A (11c7) antibody and Nogo-66-Fc binding using an anti-Fc antibody. **A.** Binding analysis of Nogo-A-Δ20 and Nogo-66 to Heparin, HS, CS-A, CS-C or CS-E. **B.** Binding analysis of Nogo-A-Δ20 and Nogo-66 to brain-derived GAGs treated with heparinase (CS-GAGs) or chondroitinase ABC (HS-GAGs). Total GAGs refer to the untreated GAG fraction. **C.** Saturation curve of Nogo-A-Δ20 to heparin (K_d ~ 234nM) and brain-derived HS-GAGs (K_d ~ 562nM). Detection was performed using the anti-T7 antibody. **D.** Scatchard plot of **C**. **E.** Representative images of cell surface binding of Nogo-A-Δ20 to CHO WT and HSPG-deficient CHO pgsD-677 cells. Cells were incubated with 1 μM HA-tagged Nogo-A-Δ20 for 30 min on ice and stained using the anti-HA antibody. **F,G.** Quantification of cell surface binding by assessing the number of bound HA-tagged Nogo-A-Δ20 spots in CHO WT and pgsD-677 cells (**F**) or in HepIII vs. saline-treated 3T3 cells (**G**). Average values for the control were subtracted from the respective measurements. Data shown are means ± SEM (**A-D**: n = 3 experiments; **F**: n = 10 cells; **G**: n = 30-34 cells). **A,B**: One-way ANOVA with Tuckey's post hoc test; **F,G**: Mann Whitney test (*** $p < 0.001$).

Figure 4. HSPGs mediate Nogo-A-Δ20 signaling independently of S1PR2. A. Cell spreading quantification of CHO WT and CHO pgsD-677 cells treated with 1 μM JTE-013 or vehicle (DMSO) and plated on a control (ctrl) or Nogo-A-Δ20 substrate. Representative pictures are shown in Figure S3A. **B.** Cell spreading quantification of WT and S1PR2$^{-/-}$ MEFs treated with 2.5 U/ml HepIII or vehicle (saline) and plated on a control (ctrl) or Nogo-A-Δ20 substrate. Representative pictures are shown in Figure S3B. **C.** RhoA activation was assessed in CHO WT and pgsD-677 cells 20 min post-incubation with 1 μM Nogo-A-Δ20 by western blotting. **D.** Quantification of RhoA-GTP/Total RhoA levels shown in **C**. Nogo-A-Δ20 does not activate RhoA in pgsD-677 cells. **E.** Representative pictures of CHO WT cells treated with the RhoA inhibitor C3 transferase (0.1 mg/ml), the ROCK blocker Y-27632 (5 μM) or vehicle (saline). **F.** Cell spreading quantification of **E**. Data shown are means ± SEM (**B,F**: n = 6-16 coverslips; **D**: n = 3 experiments. **B,D,F**: One-way ANOVA with Tuckey's post hoc test (** $p < 0.01$; *** $p < 0.001$). Scale bars: 45 μm. See also Figure S3 and S4.

Figure 5. Syndecans mediate Nogo-A-Δ20 of cell spreading and neurite outgrowth. A. qRT-PCR expression analysis of syndecans (Sdc) in 3T3 cells. mRNA fold changes are normalized to Sdc1 (100%). **B.** Representative pictures of 3T3 cells treated with a lentivirus expressing Sdc4 or ctrl shRNA for 96 h and replated on a ctrl or Nogo-A-Δ20 substrate for 1 h. Cells were stained with Phalloidin-Alexa488. **C.** Cell spreading quantification of **B**. **D.** qRT-PCR expression analysis of Sdc's in DIV4 rat E19 cortical neurons. mRNA fold changes are normalized to Sdc1 (100%). **E.** Representative pictures of DIV8 rat cortical neurons treated at DIV4 with ctrl or Sdc3 siRNA for 72 h and replated on a ctrl or Nogo-A-Δ20 substrate for 24 h. Cells were stained with MAP1b. **F.** Neurite length quantification of **E**. **G.** RhoA activation was assessed in 3T3 cells expressing Sdc4 or ctrl shRNA 20 min post-incubation with 1 μM Nogo-A-Δ20 using a commercially available ELISA kit. Quantification of RhoA-GTP/Total RhoA levels is shown. **H.** Microscale binding analysis of Nogo-A-Δ20 to

recombinant mouse Sdc4 ($K_d \sim 522.1$nM) or Sdc3 ($K_d \sim 865.7$nM). Single dots indicate biological replicates in **A** and **D**. Data shown are means ± SEM (**A,D**: n = 3 experiments; **G**: n = 6 experiments; **C,F**: n = 8-16 coverslips). **C,F,G**: One-way ANOVA with Tuckey's post hoc test (* $p < 0.05$, *** $p < 0.001$; ns: not significant). Scale bars: 45 μm. See also Figure S5.

Figure 6. Nogo-A-Δ20 regulates neuroblast adhesion and migration via HSPGs. A. Representative pictures of neuroblast explants (SVZ+RMS) showing the decrease in migration area of HepIII (500 mU/ml), 11c7 (1 μg/μl) and HepIII+11c7-treated explants vs. controls. **B.** Quantification of the migration area. Controls are set to 100% for each experiment. **C.** Adhesion of SVZ-dissociated neuroblasts on a Nogo-A-Δ20 substrate after treatment with 11c7 and/or HepIII. No synergistic activity is detected by co-treatment of neuroblasts with 11c7 and HepIII in **B** and **C**. **D.** Representative pictures of neuroblast explants (SVZ+RMS) treated with different concentrations of JTE-013 or vehicle (DMSO). **E.** Quantification of the migration in the presence of JTE-013 vs. DMSO. Controls are set to 100% for each experiment. **F.** Adhesion of SVZ-dissociated neuroblasts on a Nogo-A-Δ20 substrate after treatment with JTE-013 or DMSO. No significant effect is observed upon treatment with JTE-013 in **E** and **F**. Data shown are means ± SEM (**B**: n = 4-5 experiments; **C**: n = 3 coverslips; **E**: n = 4-5 experiments, **F**: n = 5 coverslips). **B,C,E,F**: One-way ANOVA with Bonferroni's post hoc test (* $p < 0.05$, ** $p < 0.01$, *** $p < 0.001$). Scale bars: **A**: 100 μm.

Figure 1

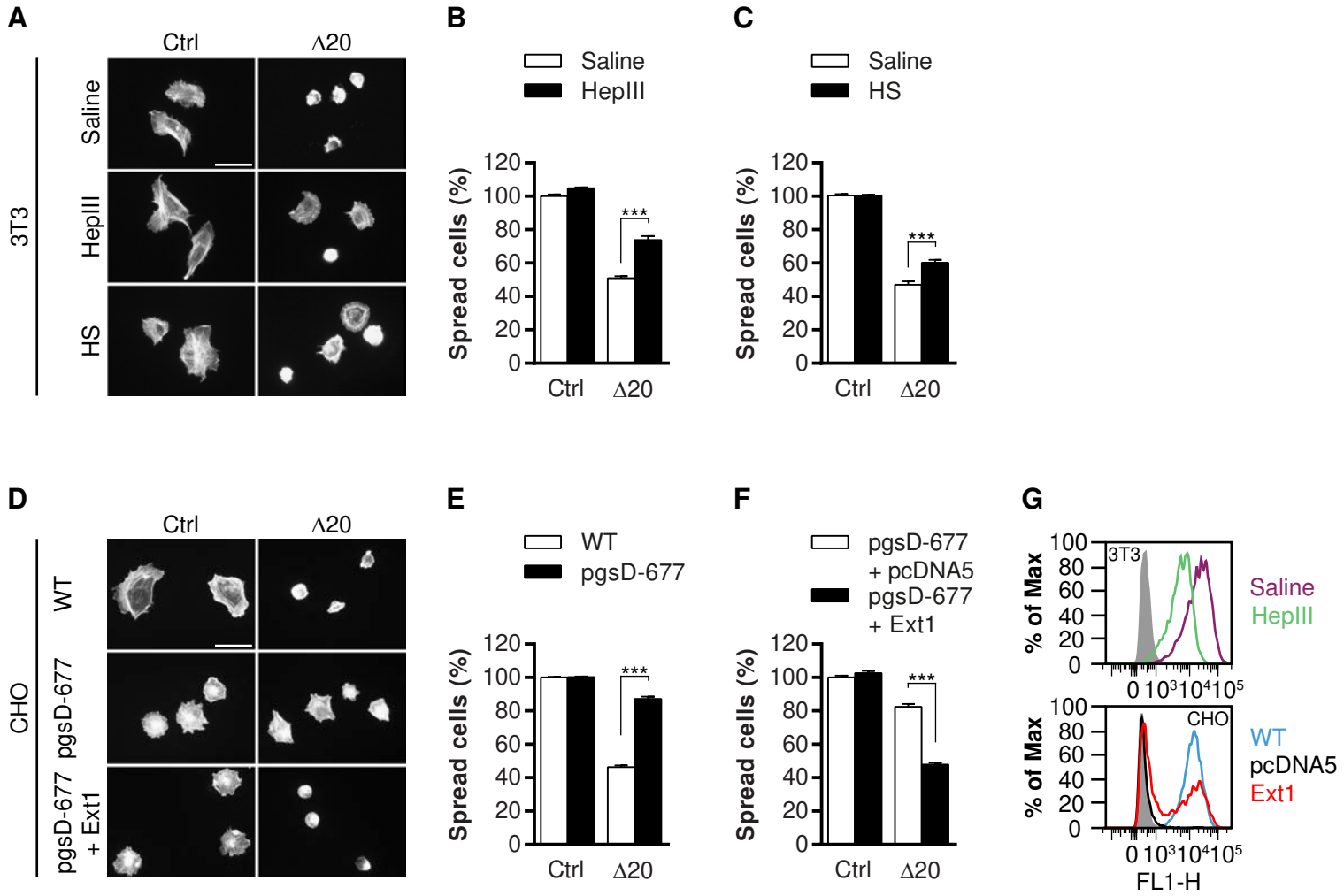
A
Ctrl
Δ20
3T3
Saline
HepIII
HS
B
Saline
HepIII
Spread cells (%)
120
100
80
60
40
20
0
***
Ctrl
Δ20
C
Saline
HS
Spread cells (%)
***
Ctrl
Δ20
D
Ctrl
Δ20
CHO
WT
pgsD-677
pgsD-677 + Ext1
E
WT
pgsD-677
Spread cells (%)
***
Ctrl
Δ20
F
pgsD-677 + pcDNA5
pgsD-677 + Ext1
Spread cells (%)
***
Ctrl
Δ20
G
% of Max
100
80
60
40
20
0
3T3
Saline
HepIII
0 10³10⁴10⁵
% of Max
CHO
WT
pcDNA5
Ext1
0 10³10⁴10⁵
FL1-H

Figure 2

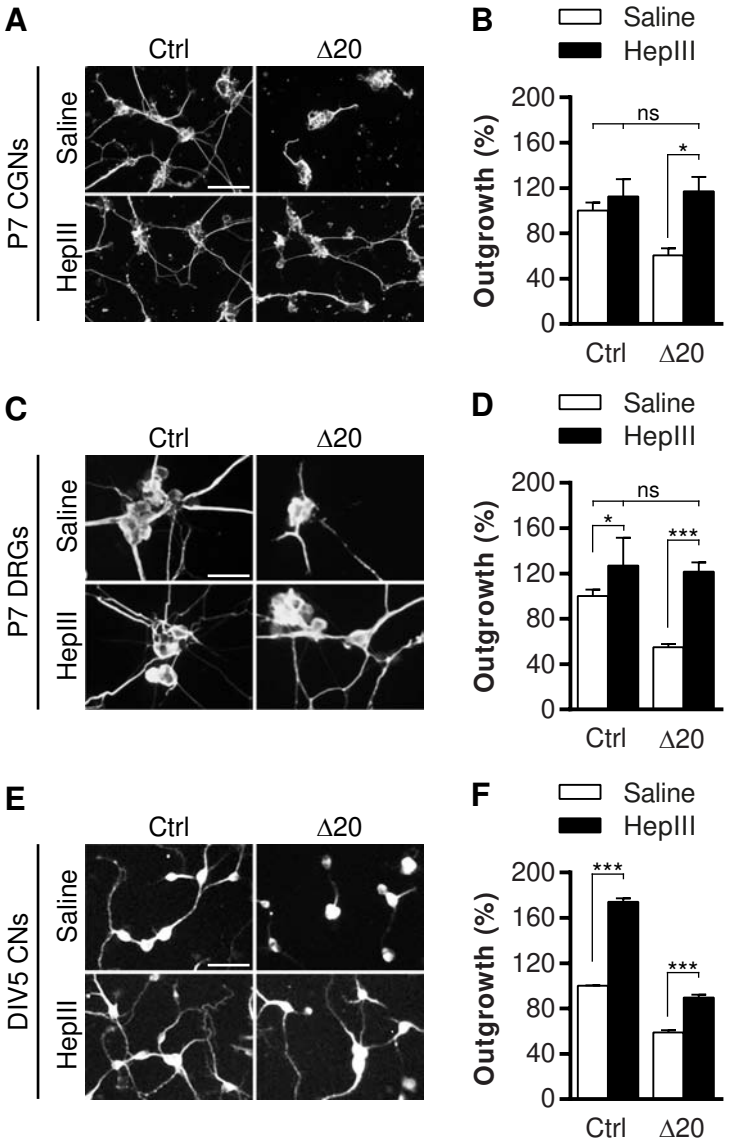
A
Ctrl
Δ20
P7 CGNs
Saline
HepIII
B
Saline
HepIII
Outgrowth (%)
200
160
120
80
40
0
ns
*
Ctrl
Δ20
C
Ctrl
Δ20
P7 DRGs
Saline
HepIII
D
Saline
HepIII
Outgrowth (%)
200
160
120
80
40
0
ns
*
***
Ctrl
Δ20
E
Ctrl
Δ20
DIV5 CNs
Saline
HepIII
F
Saline
HepIII
Outgrowth (%)
200
160
120
80
40
0
***
***
Ctrl
Δ20

Figure 3

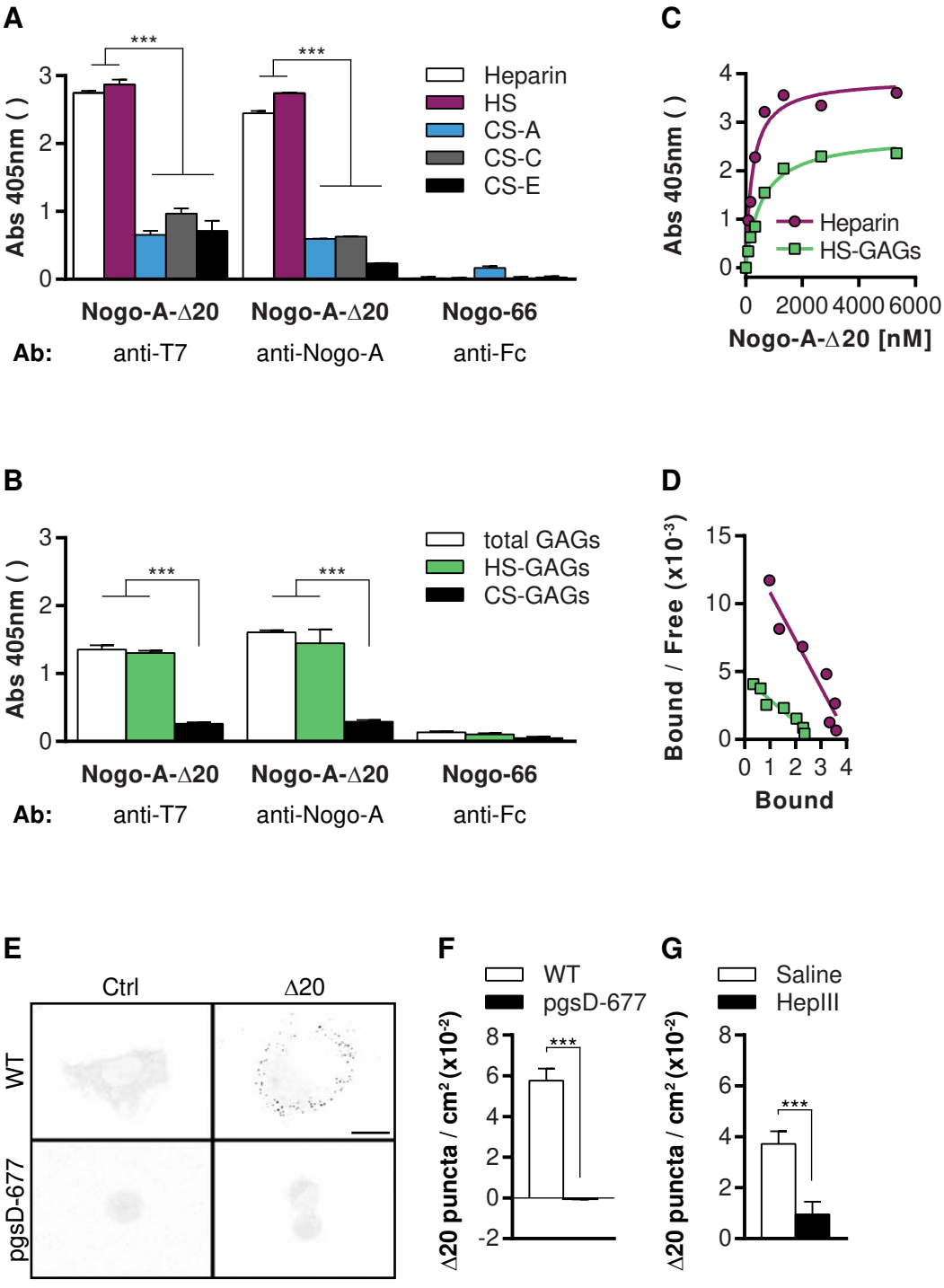
A
***
***
Heparin
HS
CS-A
CS-C
CS-E
Abs 405nm ( )
Nogo-A-Δ20
Nogo-A-Δ20
Nogo-66
Ab:
anti-T7
anti-Nogo-A
anti-Fc
C
Abs 405nm ( )
Heparin
HS-GAGs
Nogo-A-Δ20 [nM]
B
***
***
total GAGs
HS-GAGs
CS-GAGs
Abs 405nm ( )
Nogo-A-Δ20
Nogo-A-Δ20
Nogo-66
Ab:
anti-T7
anti-Nogo-A
anti-Fc
D
Bound / Free (x10-3)
Bound
E
Ctrl
Δ20
WT
pgsD-677
F
WT
pgsD-677
***
Δ20 puncta / cm2 (x10-2)
G
Saline
HepIII
***
Δ20 puncta / cm2 (x10-2)

Figure 4

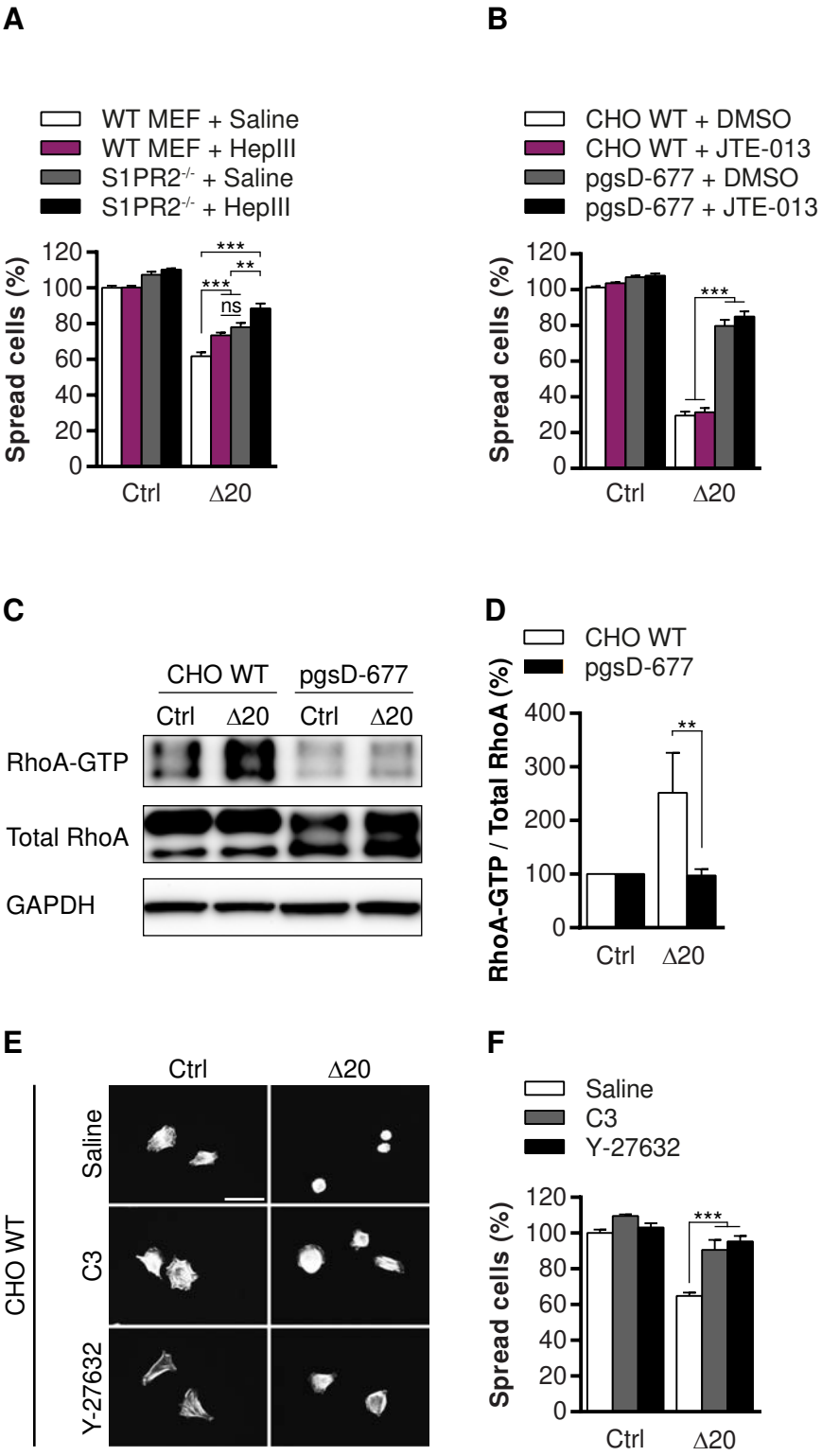
A
WT MEF + Saline
WT MEF + HepIII
S1PR2-/- + Saline
S1PR2-/- + HepIII
Spread cells (%)
120
100
80
60
40
20
0
***
**
***
ns
Ctrl
Δ20
B
CHO WT + DMSO
CHO WT + JTE-013
pgsD-677 + DMSO
pgsD-677 + JTE-013
Spread cells (%)
120
100
80
60
40
20
0
***
Ctrl
Δ20
C
CHO WT
pgsD-677
Ctrl
Δ20
Ctrl
Δ20
RhoA-GTP
Total RhoA
GAPDH
D
CHO WT
pgsD-677
RhoA-GTP / Total RhoA (%)
400
300
200
100
0
**
Ctrl
Δ20
E
Ctrl
Δ20
CHO WT
Saline
C3
Y-27632
F
Saline
C3
Y-27632
Spread cells (%)
120
100
80
60
40
20
0
***
Ctrl
Δ20

Figure 5

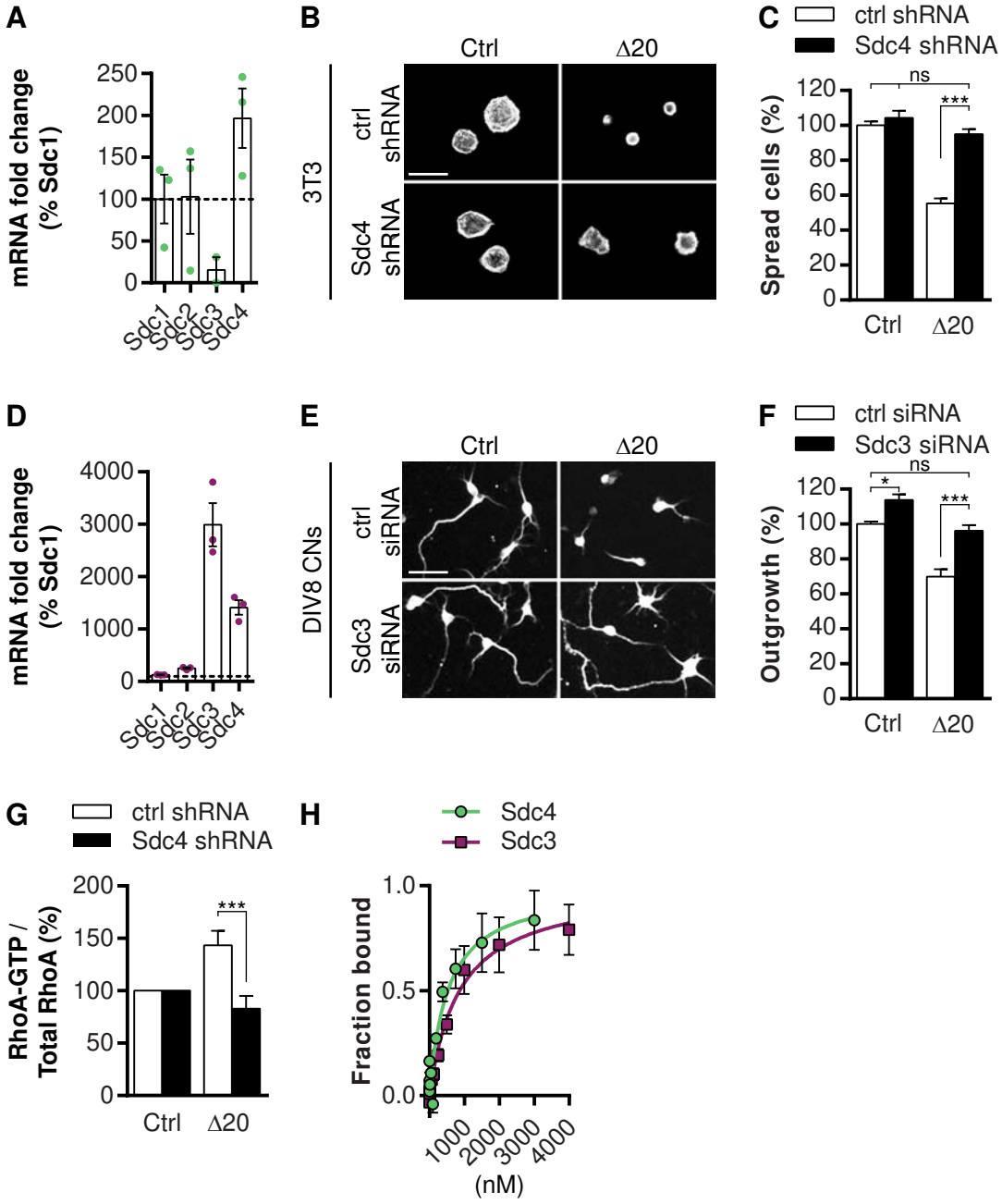
A
mRNA fold change (% Sdc1)
250
200
150
100
50
0
Sdc1
Sdc2
Sdc3
Sdc4
B
Ctrl
Δ20
3T3
ctrl shRNA
Sdc4 shRNA
C
ctrl shRNA
Sdc4 shRNA
Spread cells (%)
120
100
80
60
40
20
0
ns
***
Ctrl
Δ20
D
mRNA fold change (% Sdc1)
4000
3000
2000
1000
0
Sdc1
Sdc2
Sdc3
Sdc4
E
Ctrl
Δ20
DIV8 CNs
ctrl siRNA
Sdc3 siRNA
F
ctrl siRNA
Sdc3 siRNA
Outgrowth (%)
120
100
80
60
40
20
0
ns
*
***
Ctrl
Δ20
G
ctrl shRNA
Sdc4 shRNA
RhoA-GTP / Total RhoA (%)
200
150
100
50
0
***
Ctrl
Δ20
H
Sdc4
Sdc3
Fraction bound
1.0
0.5
0.0
1000
2000
3000
4000
(nM)

Figure 6

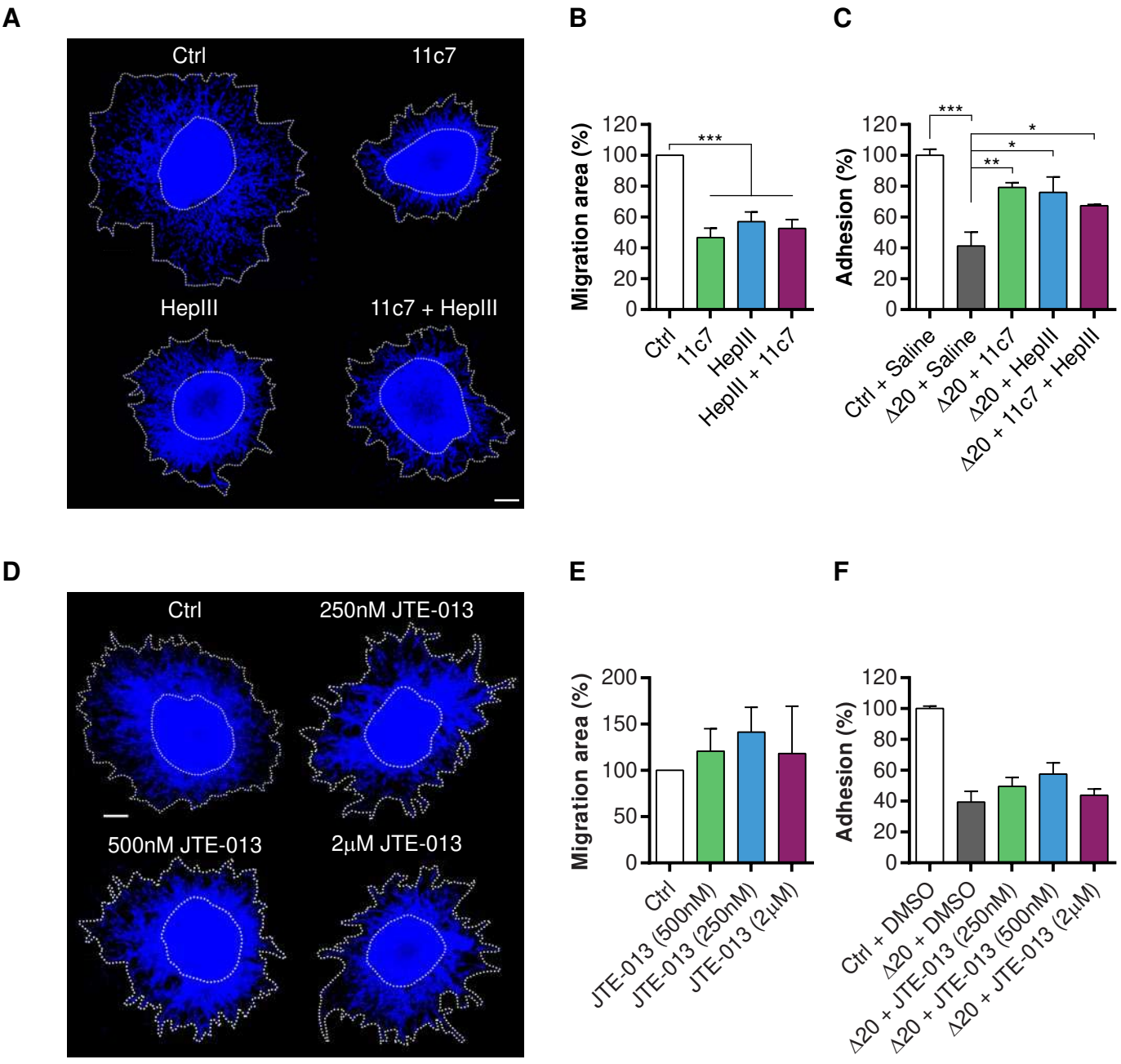
A
Ctrl
11c7
HepIII
11c7 + HepIII
B
Migration area (%)
120
100
80
60
40
20
0
***
Ctrl
11c7
HepIII
HepIII + 11c7
C
Adhesion (%)
120
100
80
60
40
20
0
***
*
*
**
Ctrl + Saline
Δ20 + Saline
Δ20 + 11c7
Δ20 + HepIII
Δ20 + 11c7 + HepIII
D
Ctrl
250nM JTE-013
500nM JTE-013
2μM JTE-013
E
Migration area (%)
200
150
100
50
0
Ctrl
JTE-013 (500nM)
JTE-013 (250nM)
JTE-013 (2μM)
F
Adhesion (%)
120
100
80
60
40
20
0
Ctrl + DMSO
Δ20 + DMSO
Δ20 + JTE-013 (250nM)
Δ20 + JTE-013 (500nM)
Δ20 + JTE-013 (2μM)

Figure S1

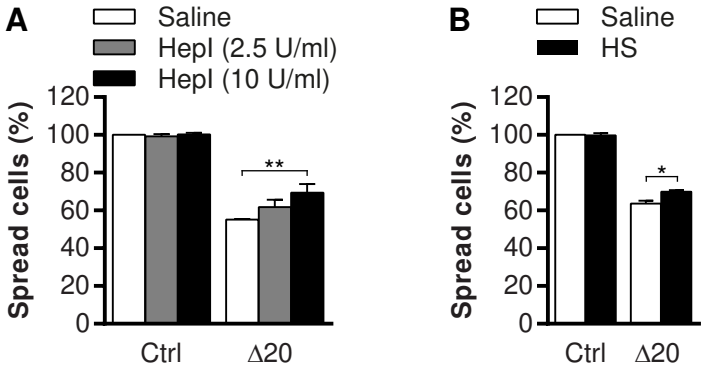

Figure S1. Related to Figure 1. Effect of HepI treatment and pre-incubation of HS and Nogo-A-Δ20 on Nogo-A-Δ20-induced inhibition of cell spreading. **A.** Cell spreading quantification of 3T3 fibroblasts treated with 2.5 U/ml HepI, 10 U/ml HepI or vehicle (saline) and plated on control (ctrl) and Nogo-A-Δ20 substrates. **B.** Cell spreading quantification of 3T3 fibroblasts plated on a substrate consisting of Nogo-A-Δ20 pre-incubated with HS (0.1 mg/ml). Data shown are means ± SEM (**A,B**: n = 3-6 coverslips). **A,B**: One-way ANOVA with Tuckey's post hoc test (* $p < 0.05$, ** $p < 0.01$).

Figure S2

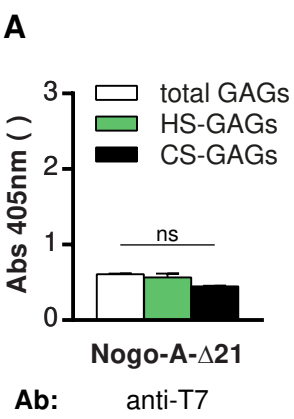

Figure S2. Related to Figure 3. Binding of Nogo-A-Δ21 to brain-derived GAGs. **A**. Biotinylated brain-derived GAGs treated with heparinase (CS-GAGs) or chondroitinase ABC (HS-GAGs) or untreated (total GAGs) were coated onto streptavidin-coated wells and analysed for Nogo-A-Δ21 binding by an ELISA-type assay. Average values for the BSA negative control were substracted from the respective readings. Nogo-A-Δ21-T7 binding was detected using an anti-T7 antibody. Data shown are means ± SEM (**A,B**: n = 3 experiments). **A**: One-way ANOVA with Tuckey's post hoc test (ns: not significant).

Figure S3

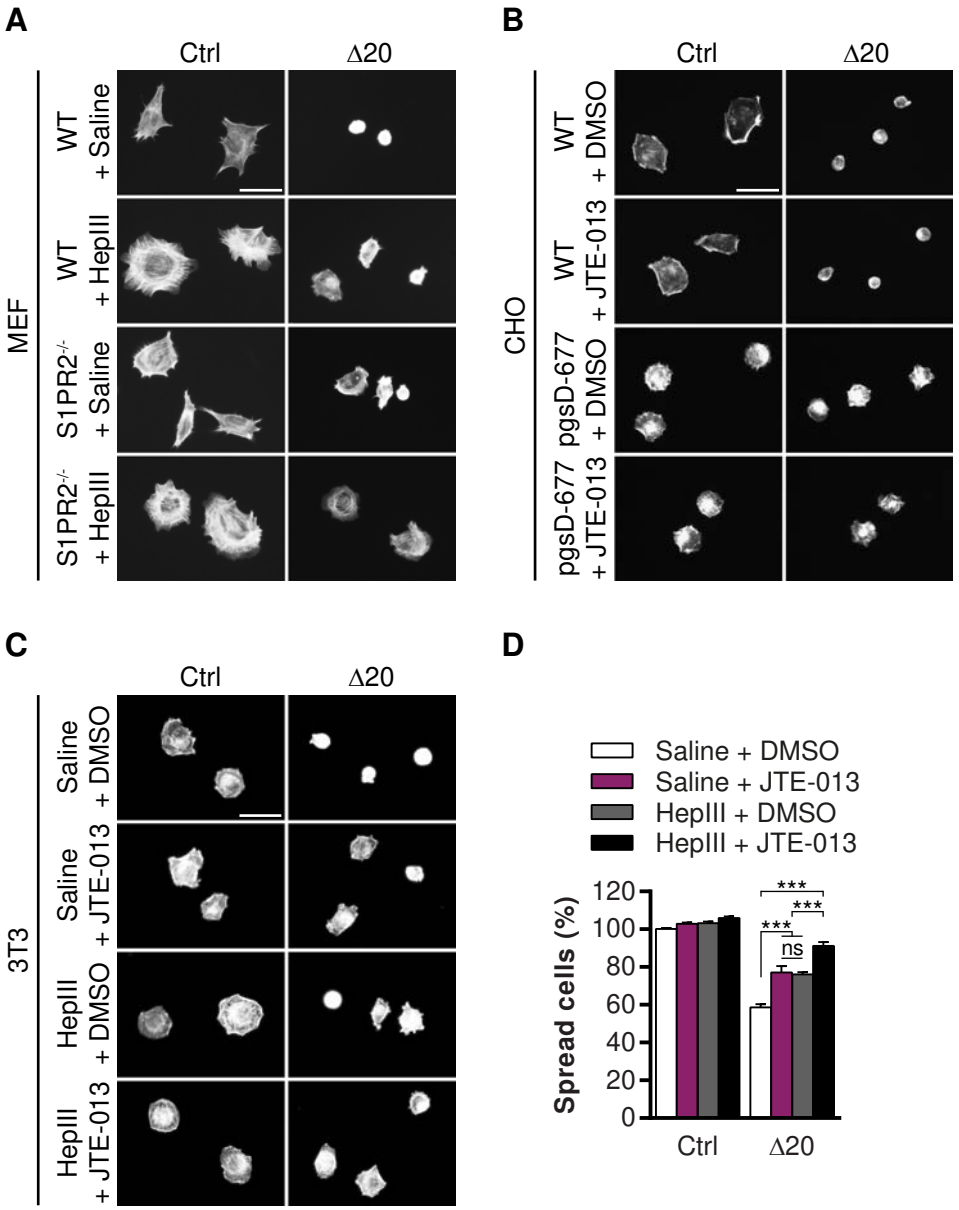

Figure S3. Related to Figure 4. Effects of S1PR2 blockade/knockout and HepIII treatment. **A.** Representative pictures of WT and S1PR2$^{-/-}$ MEFs treated with 2.5 U/ml HepIII or vehicle (saline) and plated on control (ctrl) and Nogo-A-Δ20 substrates. **B.** Representative pictures of CHO WT and CHO pgsD-677 cells treated with 1 μM JTE-013 or vehicle (DMSO) and plated on control (ctrl) and Nogo-A-Δ20 substrates. Quantification of **A** and **B** is shown in Figure 4A and 4B. **C.** Representative pictures of 3T3 cells treated with 2.5 U/ml HepIII or vehicle (saline) and plated on a control (ctrl) or Nogo-A-Δ20 substrate in the presence of 1 μM JTE-013 or vehicle (DMSO). **D.** Co-treatment with HepIII and JTE-013 led to an additive effect on Nogo-A-Δ20 inhibition rescue in 3T3 cells. Data shown are means ± SEM (**B,D**: n = 5-9 coverslips). **B,D**: One-way ANOVA with Tuckey's post hoc test (** $p < 0.01$; *** $p < 0.001$; ns: not significant). Scale bars: 45 μm.

Figure S4

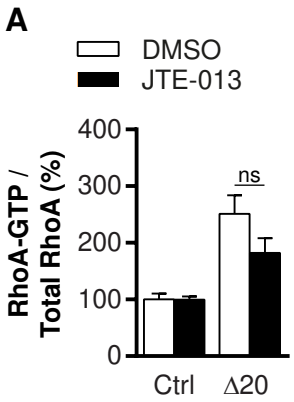

Figure S4. Related to Figure 4. JTE-013 treatment does not affect RhoA activation in S1PR2-negative CHO cells. **A.** RhoA activation was assessed in CHO WT cells 20 min post-incubation with 1 μM Nogo-A-Δ20 using an ELISA kit. Data shown are means ± SEM (n = 3 experiments). Mann Whitney test (ns: not significant).

Figure S5

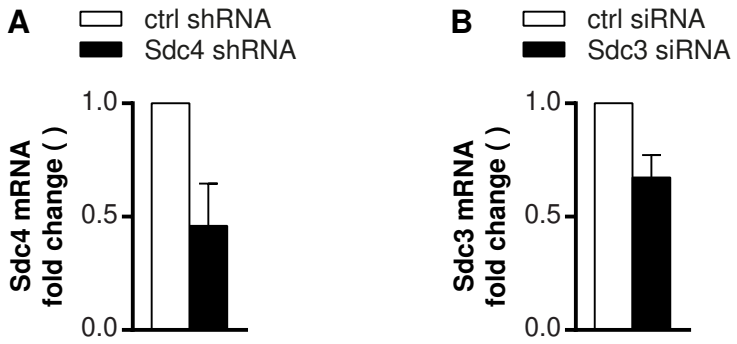

Figure S5. Related to Figure 5. Knockdown efficiency of syndecan shRNA and siRNA constructs. **A.** Quantitative RT-PCR analysis of 3T3 cells expressing lentivirally delivered syndecan-4 (Sdc4) shRNA for 96 h. Scrambled shRNA (ctrl) was used as control and set to 1. Relative quantification of expression levels: Sdc4 (0.460 ± 0.186). **B.** Quantitative RT-PCR analysis of E19 cortical neurons treated at DIV4 with syndecan-3 (Sdc3) or scrambled (ctrl) siRNA for 72 h. Scrambled siRNA was set to 1. Relative quantification of expression levels: Sdc3 (0.673 ± 0.099). Data shown are means ± SEM (**A,B**: n = 3-4 experiments).

Supplemental Figure Legends

Figure S1. Related to Figure 1. Effect of HepI treatment and pre-incubation of HS and Nogo-A-Δ20 on Nogo-A-Δ20-induced inhibition of cell spreading. A. Cell spreading quantification of 3T3 fibroblasts treated with 2.5 U/ml HepI, 10 U/ml HepI or vehicle (saline) and plated on control (ctrl) and Nogo-A- Δ20 substrates. **B.** Cell spreading quantification of 3T3 fibroblasts plated on a substrate consisting of Nogo-A- Δ20 pre-incubated with HS (0.1 mg/ml). Data shown are means ± SEM (**A,B**: n = 3-6 coverslips). **A,B**: One-way ANOVA with Tuckey's post hoc test (* $p < 0.05$, ** $p < 0.01$).

Figure S2. Related to Figure 3. Binding of Nogo-A-Δ21 to brain-derived GAGs. A. Biotinylated brain-derived GAGs treated with heparinase (CS-GAGs) or chondroitinase (HS-GAGs) or untreated (total GAGs) were coated onto streptavidin-coated wells and analysed for Nogo-A-Δ21 binding by an ELISA-type assay. Average values for the BSA negative control were substracted from the respective readings. Nogo-A-Δ21-T7 binding was detected using an anti-T7 antibody. Data shown are means ± SEM (**A,B**: n = 3 experiments). **A**: One-way ANOVA with Tuckey's post hoc test (ns: not significant).

Figure S3. Related to Figure 4. Effects of S1PR2 blockade/knockout and HepIII treatment. A. Representative pictures of WT and S1PR2$^{-/-}$ MEFs treated with 2.5 U/ml HepIII or vehicle (saline) and plated on control (ctrl) and Nogo-A-Δ20 substrates. **B**. HepIII treatment of S1PR2$^{-/-}$ MEFs led to an additive effect on Nogo-A-Δ20 inhibition rescue as opposed to S1PR2 knockout or HepIII treatment alone. **C**. Representative pictures of 3T3 cells treated with 2.5 U/ml HepIII or vehicle (saline) and plated on a control (ctrl) or Nogo-A-Δ20 substrate in the presence of 1 μM JTE-013 or vehicle (DMSO). **D.** Co-treatment with HepIII and JTE-013 led to an additive effect on Nogo-A-Δ20 inhibition rescue in 3T3 cells. Data shown are means ± SEM (**B,D**: n = 5-9 coverslips). **B,D**: One-way ANOVA with Tuckey's post hoc test (** $p < 0.01$; *** $p < 0.001$; ns: not significant). Scale bars: 45 μm.

Figure S4. Related to Figure 4. JTE-013 treatment does not affect RhoA activation in S1PR2-negative CHO cells. RhoA activation was assessed in CHO WT cells 20 min post-incubation with 1 μM Nogo-A-Δ20 using an ELISA kit. Data shown are means ± SEM (n = 3 experiments). Mann Whitney test (ns: not significant).

Figure S5. Related to Figure 5. Knockdown efficiency of syndecan shRNA and siRNA constructs. A. Quantitative RT-PCR analysis of 3T3 cells expressing lentivirally delivered syndecan-4 (Sdc4) shRNA for 96 h. Scrambled shRNA (ctrl) was used as control and set to 1. Relative quantification of expression levels: Sdc4 (0.460 ± 0.186). **B.** Quantitative RT-PCR analysis of E19 cortical neurons treated at DIV4 with syndecan-3 (Sdc3) or scrambled (ctrl) siRNA for 72 h. Scrambled siRNA was set to 1. Relative quantification of expression levels: Sdc3 (0.673 ± 0.099). Data shown are means ± SEM (**A,B**: n = 3-4 experiments).

Supplemental Experimental Procedures

Recombinant fusion proteins, reagents and antibodies

Recombinant proteins Nogo-A-Δ20 (rat aa544-725) and Nogo-A-Δ21 (rat aa812-918) were purified as described previously (Oertle et al., 2003). Briefly, BL21/DE3 *E. coli* were transformed with the pET28 expression vector (Novagen) containing His-/T7-tagged Nogo-A-Δ20, His-/T7-tagged Nogo-A-Δ21 or His-/HA-tagged Nogo-A-Δ20 and cultured at 37°C to reach an OD of 0.6 AU. Protein expression was induced by addition of 1 M IPTG for 2 h at 30°C. Fusion proteins were purified using Co^{2+}-Talon Metal Affinity Resin (Takara Bio Inc.).

CS variants and HS were purchased from Seikagaku Corp (Japan) where CS-A is isolated from whale cartilage, CS-C is from shark cartilage, CS-E is from squid cartilage and HS is from bovine kidney. The biotinylated-heparin isolated from porcine intestine was purchased from Sigma.

The following primary antibodies were used: mouse anti-βIII Tubulin (Promega G712A, clone 5G8; ICC: 1:1000), 4',6-diamidino-2-phenylindole (DAPI) (Invitrogen D1306; ICC: 1:1000), mouse anti-GAPDH (Abcam, ab8245; 1:20,000), rat anti-HA tag (Roche 11867423001; ICC: 1:200), mouse anti-heparan sulfate (Seikagaku Corp 370255-1, clone F58-10E4; FACS: 1 µg/10^6 cells), mouse IgM isotype control (BD Pharmingen 557275, clone C48-6; FACS: 1 µg/10^6 cells), goat anti-mouse IgG, Fcγ fragment specific (Jackson Immunoresearch 115-005-071; ELISA: 1 µg/ml), mouse anti-Map-1b (Santa Cruz sc-58784, clone AA6; ICC 1:2000), mouse anti-Nogo-A (11c7, (Oertle et al., 2003), ELISA: 1 µg/ml), Phalloidin-Alexa488 (Invitrogen A12379; ICC: 1:500), rabbit anti-RhoA (Cell Signaling 2117; WB: 1:1000), mouse anti-T7 tag (Novagen 69522-3; ELISA: 1 µg/ml).

The following secondary antibodies were used: goat anti-mouse IgG Alexa488-conjugated (Invitrogen A11029; ICC: 1:1000), rat anti-mouse IgM FITC-conjugated (BD Pharmingen 553437, clone II/41; FACS: 1:1000), HRP-conjugated goat anti-rabbit IgG (Jackson Immunoresearch).

Brain derived glycosaminoglycans (GAGs)

Adult Sprague Dawley rats were sacrificed and decapitated. The brains were cut into smaller pieces before de-lipidation with cold acetone. The tissues were then dried and homogenized in cold pronase buffer. The brain was then treated with pronase overnight and the proteins/peptides were removed by precipitation using trichloroacetic acid, followed by centrifugation. The residual trichloroacetic acid retained in the supernatant (which contains the GAGs) is removed with 5 diethyl ether washes. The GAGs were precipitated with sodium acetate and absolute ethanol overnight at 4°C and recovered after centrifugation. The resulting pellet will be reconstituted in 500 µl of de-ionized water and stored at -20°C.

Tissue preparation and cell culture

Total myelin protein extracts were prepared from the spinal cords of adult Wistar rats as described previously (Oertle et al., 2003). Swiss 3T3 (ATCC) cells and primary mouse embryonic fibroblasts (MEFs) were maintained in Dulbecco's modified eagle medium (DMEM) (Sigma, Invitrogen) containing 10% neonatal calf serum (Invitrogen). CHO K1 WT (ATCC) and CHO pgsD-677 cells (ATCC) were maintained in DMEM containing 10% fetal bovine serum (FBS) (Invitrogen). Primary $S1PR2^{-/-}$ MEFs were described previously (Kempf et al., 2014). P5-8 mouse CGNs, P5-8 mouse DRG neurons and E19 rat cortical neurons were prepared as described previously (Kempf et al., 2014; Oertle et al., 2003). HEK293T (ATCC) cells were maintained in Iscove's modified Dulbecco's medium (IMDM) (Life Technologies) medium supplemented with 4 mM L-Glutamine (Sigma), 1% Penicillin/Streptomycin (Pen/Strep) (Life Technologies) and 10% FBS. Swiss 3T3 ctrl shRNA and Sdc4 shRNA cells were selected with 4µg/mL puromycin. All cell lines and primary cells were cultured at 37°C and 5% CO2.

Immunocytochemistry

Cell lines and primary cells were fixed with 4% paraformaldehyde (PFA) for 15 min, washed and permeabilized with 0.1% Triton X-100. After blocking with 2% goat serum, cells were first incubated with the primary antibodies for 30 min at room temperature and detected using corresponding secondary antibodies in 2% goat serum.

For cell surface immunocytochemical detection of Nogo-A-Δ20, cells were first incubated with 1 µM HA-tagged Nogo-A-Δ20 and subsequently with anti-HA antibodies for 1 h each on ice in serum-free medium containing 0.02% sodium azide (Sigma). Cells were washed, fixed with 1% PFA and stained with secondary antibodies. Image stacks were acquired using a Leica SP5 confocal microscope equipped with a 63x oil immersion objective (NA 1.4). Stacks were reconstructed in 3D with Imaris (Bitplane) and the cell surface area was measured for each cell. Bound Nogo-A-Δ20 puncta were counted using the spot function of Imaris and the total number was normalized to the cell surface area for each cell. The average ratio obtained with secondary antibody only controls was baseline-subtracted from each cell.

Flow cytometry

For FACS analysis, non-fixed cells were detached using 0.05% Trypsin/EDTA (Invitrogen), washed 1x in PBS, washed 2x in Tris-Buffer/1%BSA at 4°C and stained with the indicated primary antibodies followed by fluorescently-conjugated secondary antibodies for 30 min each in Tris-Buffer/5%BSA on ice. Cells were immediately analyzed by FACS (BD Canto II). FACS staining was quantitated using the FlowJo (Tree Star Inc) software. The fluorescence intensity is displayed on the X-axis (divided into 256 bins). The % of Max on the Y-axis stands for the number of cells in each bin on the X-axis (FlowJo uses an arbitrary number of 256 bins) divided by the number of cells in the bin that contains the largest number of cells.

RhoA activation assays

3T3 cells were serum-starved overnight and treated for 20 min with 1 µM Nogo-A-Δ20 or Nogo-A-Δ21 control protein. Pulldown of activated RhoA-GTP was subsequently performed using the RhoA Activation Assay Biochem Kit according to the manufacturer's instructions (Cytoskeleton, Inc.). Alternatively, RhoA activation was assessed using the total RhoA ELISA and RhoA G-LISA kit according to the manufacturer's instructions (Cytoskeleton, Inc.). Levels of activated RhoA were normalized to total RhoA levels for each biological replicate.

***In vitro* bioassays**

3T3 fibroblast spreading assays and neurite outgrowth assays were performed as described previously (Kempf et al., 2014; Oertle et al., 2003). Briefly, 4-well plates (Greiner) were coated with 40-100 pmol/cm^2 (0.4-1 µM) Nogo-A-Δ20 or Nogo-A-Δ21 (control protein) or 5 µg/cm^2 myelin at 4°C overnight. In outgrowth experiments, wells were precoated with 0.3 µg/ml Poly-L-Lysine (PLL; Sigma) for 1 h at 37°C before the addition of the different substrates. Unbound material was removed by three washes with PBS. Cell lines were detached with 2% (w/v) EDTA in PBS and plated at 7000 cells per cm^2 for 1 h at 37°C and 5% CO2, fixed with 4% PFA and stained with Phalloidin-Alexa488. For HepI and HepIII (Sigma) treatment, cells were incubated with 2.5 U/ml HepIII or 2.5-10 U/ml HepI 3 h prior plating and during the spreading assay. Higher concentrations of HepIII could not be used under our experimental conditions because of their effects on cell viability. For JTE-013 (Tocris), Y-27632 (Sigma) and cell-permeable C3 transferase (CT04, Cytoskeleton), cells were incubated with 1 µM JTE-013, 5 µM Y-27632 or 100 µg/ml C3 30 min prior plating and during the spreading assay. The corresponding solvents or isotype antibodies were used as controls. For expression of EXT1 in pgsD-677 cells, pgsD-677 cells were transfected with Ext1 cDNA using Lipofectamine 2000 (Invitrogen) 48 h prior replating according to the manufacturer's instructions. The percentage of cells that remained round i.e. did not spread was quantified manually in four randomly chosen areas of the well/coverslip and averaged over those areas (n = 1 coverslip). Data were normalized to baseline and plotted as mean ± SEM from multiple biological replicates.
CGNs were plated at 7.5x10^4 cells per cm^2, DRGs at 7.5x10^3 cells per cm^2 and cortical neurons at 5x10^4 cells per cm^2 onto the various substrates. Neurons were cultured for 24-48 h at 37°C and 5% CO2, fixed with 4% PFA and stained with anti-βIII Tubulin (CGNs and DRGs) or Mab1b (cortical neurons). Treatment of CGNs with 500 mU/ml HepIII and DRGs with 1 U/ml HepIII started 12 h post-plating until fixation. Cortical neurons were treated at DIV4 with 1 U/ml HepIII for 3 h and replated for 24 h in the presence of HepIII. The corresponding solvents were used as control. Neurons were imaged with an Axioskop 2 microscope (Zeiss) equipped with a Plan-NEOFLUAR 10X/NA 0.3 objective in a semi-automated way. Mean total neurite length per cell was quantified using the MetaMorph software (Molecular Devices) in four randomly chosen areas of the well/coverslip and averaged over those areas (n = 1 coverslip). Data were normalized to baseline and plotted as mean ± SEM from multiple biological replicates.

siRNA/shRNA

E19 rat cortical neurons were plated at 0.6x10^6 cells in 6-well plates coated with 0.3 µg PLL and transfected at DIV4 with 50 nM siRNA using DharmaFECT 3 (Dharmacon) according to the manufacturer's instructions. Three days post-transfection, neurons were detached with 0.25% Trypsin and replated on a Nogo-A-Δ20 or control substrate for 24 h as described above. Swiss 3T3 cells were plated at 2.9x10^4 in 24-well plates and transfected with 50 nM siRNA using DharmaFECT 3 (Dharmacon) according to the manufacturer's instructions. 3 days post-transfection, cells were replated on a Nogo-A-Δ20 or control substrate for 1 h. Following siRNAs were used: rat Syndecan-3 ON-TARGETplus SMARTpool Sdc3 siRNA (L-098896-02-0005), mouse Glypican-1 ON-TARGETplus SMARTpool Gpc1 siRNA (L-049268-01-0005), mouse Glypican-4 ON-TARGETplus SMARTpool Gpc4 siRNA (L-045841-01-0005), mouse Glypican-6 ON-TARGETplus SMARTpool Gpc6 siRNA (L-049420-01-0005) and ON-TARGETplus siRNA non-targeting pool (D-001810-10-0005) (Thermo Scientific, Dharmacon). Quantification of the respective mRNA knockdown was performed by qRT-PCR.

The following Mission shRNA (Sigma) pLKO lentiviral plasmids containing shRNA against mouse Syndecan-4 and non-target shRNA were used for the generation of Swiss 3T3 ctrl and Sdc4 shRNA stable cell lines: TRCN0000331554 and SHC202 (TRC2 vector). Lentiviral plasmids were transfected into HEK293T cells using PEI (polyethyleimine) 25 kDa (Polysciences Inc.). Lentiviruses were concentrated from filtered culture media

(0.45 µm) by ultracentrifugation at 25000 rpm for 2 h. Quantification of the respective mRNA knockdown was performed by qRT-PCR.

Quantitative real-time PCR (qRT-PCR)

Total RNA was isolated with the RNeasy Micro kit (Qiagen) and reverse-transcribed using TayMan Reverse Transcription Reagents (Applied Biosystems). cDNA was amplified using the Light Cycler 480 thermocycler (Roche) with the polymerase ready mix (SYBR Green I Master, Roche). Relative quantification was performed using the comparative CT method. cDNA levels were normalized to the reference genes *Gapdh* and *Rpl19* (mouse) or *Gapdh* and *eF1a1* (rat). Each reaction was done in triplicate. Melting curve analysis of PCR products followed by gel electrophoresis was performed to verify amplicons. Following primers were used:

mouse *Gapdh*_FWD: 5'- CAGCAATGCATCCTGCACC -3',
mouse *Gapdh*_REV: 5'- TGGACTGTGGTCATGAGCCC -3';
mouse *Rpl19*_FWD: 5'- TGAGTATGCTCAGGCTACAG -3',
mouse *Rpl19*_REV: 5'- GAATGGACAGTCACAGGCTT -3';
mouse *Sdc4*_FWD: 5'- TTCTGGAGATCTGGATGACAC -3',
mouse *Sdc4*_REV: 5'- CACCAAGGGCTCAATCAC -3';
mouse *Gpc1*_FWD: 5'- ACTCCATGGTGCTCATCACTGAC -3',
mouse *Gpc1*_REV: 5'- TTCCACAGGCCTGGATGACCTTAG -3';
mouse *Gpc4*_FWD: 5'- ACCGACTGGTTACTGATGTCAAGG -3',
mouse *Gpc4*_REV: 5'- TTGCAAACGGTGCTTGGGAGAG -3';
mouse *Gpc6*_FWD: 5'- : GTCAGCAAAGGTCTTTCAGG -3',
mouse *Gpc6*_REV: 5'- GGTCTTTCCTCAGGGTTGTAG -3';
rat *Gapdh*_FWD: 5'- CTCTCTGCTCCTCCCTGTTC -3',
rat *Gapdh*_REV: 5'- GCCAAATCCGTTCACACC -3';
rat *eF1 1*_FWD: 5'- GCCACCATACAGTCAGAAGAG -3',
rat *eF1 1*_REV: 5'- GAACCACGGCATATTAGCAC -3'.
rat *Sdc3*_FWD: 5'- TCCACGACAATGCCATCGACTC -3',
rat *Sdc3*_REV: 5'- ACCTACGATCACAGCTACGAGCAC -3';

ELISA

The ELISA was modified according to method described in (Purushothaman et al., 2007). Biotinylated GAGs (0.5 µg per well) were immobilized onto a streptavidin-coated 384-well-plate (Pierce/Thermo scientific, IL, USA). Biotinylation of GAGs was performed by EDC and biotin-LC-hydrazide conjugation (Pierce/Thermo Scientific). After biotinylated GAGs were immobilized on the plates, the plates were blocked in 1% BSA and subjected to the binding of recombinant Nogo-66-Fc or Nogo-A-Δ20. The bound Nogo variants were then recognized by the anti-T7, anti-Fc or 11C7 antibodies. The bound antibodies were detected using anti-mouse-alkaline phosphatase conjugated antibodies followed by a direct measurement of absorbance at 405 nm using p-nitrophenylphosphate (Sigma Aldrich). BSA only controls (no recombinant proteins) measurements were used as baseline in every experiment and subtracted from the other readings. For quantification, the mean ± SEM of absorbance measurements was determined from three experiments.

Explant assay

P5 explants were prepared from C57/BL6 pups according to (Wichterle et al., 1997). Tissues from the SVZ and RMS were embedded in 75% Matrigel growth factor reduced (BD Biosciences) and maintained for 1 day in Neurobasal medium (Invitrogen) supplemented with B27 (1x; Miltenyi), Pen/Strep (20 U/ml; Sigma), and 0.5 mM glutamine (Invitrogen). Antibodies and compounds were mixed with Matrigel: 11C7 (Oertle et al., 2003), 1 µg/µl; mouse anti-human IgG, 1 µg/µl (Jackson ImmunoResearch); HepIII, 500 mU/ml (Sigma); JTE-013, 250nM, 500nM or 2µM (Tocris). Only vital explants with cells moving out of the tissue core in chains were analyzed. Explants were fixed in 4% PFA for 40, 1 µg/µl min and stained using 4',6-diamidino-2-phenylindole (DAPI; Fluka) to visualize cell nuclei or labeled for βIII Tubulin or Doublecortin (Rolando et al., 2012) to mark neuroblasts.

For adhesion experiments, adult SVZs were dissociated and SVZ-cells were either plated on poly-D-lysine (PDL) only or Nogo-A–Δ20-coated coverslips (12,000 cells/cm^2 in DMEM/F-12 supplemented with B27) (Rolando et al., 2012). Briefly, glass coverslips (1cm^2) were first coated with PDL (5 µg/ml) and then with Nogo-A–Δ20 (100 pmol/cm^2). Cells were pre-incubated with HepIII and/or 11c7 or with JTE-013 for 30 min and subsequently plated for 1 h. Cells were fixed, stained with DAPI and for βIII Tubulin and scored. The average number of adhered cells was determined by counting in five randomly chosen fields of view of the coverslips.

Supplemental References

Kempf, A., B. Tews, M.E. Arzt, O. Weinmann, F.J. Obermair, V. Pernet, M. Zagrebelsky, A. Delekate, C. Iobbi, A. Zemmar, Z. Ristic, M. Gullo, P. Spies, D. Dodd, D. Gygax, M. Korte, and M.E. Schwab. 2014. The sphingolipid receptor S1PR2 is a receptor for Nogo-a repressing synaptic plasticity. *PLoS Biol*. 12:e1001763.

Oertle, T., M.E. van der Haar, C.E. Bandtlow, A. Robeva, P. Burfeind, A. Buss, A.B. Huber, M. Simonen, L. Schnell, C. Brosamle, K. Kaupmann, R. Vallon, and M.E. Schwab. 2003. Nogo-A inhibits neurite outgrowth and cell spreading with three discrete regions. *J Neurosci*. 23:5393-406.

Purushothaman, A., J. Fukuda, S. Mizumoto, G.B. ten Dam, T.H. van Kuppevelt, H. Kitagawa, T. Mikami, and K. Sugahara. 2007. Functions of chondroitin sulfate/dermatan sulfate chains in brain development. Critical roles of E and iE disaccharide units recognized by a single chain antibody GD3G7. *J Biol Chem*. 282:19442-52.

Rolando, C., R. Parolisi, E. Boda, M.E. Schwab, F. Rossi, and A. Buffo. 2012. Distinct roles of nogo-a and nogo receptor 1 in the homeostatic regulation of adult neural stem cell function and neuroblast migration. *J Neurosci*. 32:17788-99.

Wichterle, H., J.M. Garcia-Verdugo, and A. Alvarez-Buylla. 1997. Direct evidence for homotypic, glia-independent neuronal migration. *Neuron*. 18:779-91.